

Earth's Future

RESEARCH ARTICLE

10.1029/2020EF001480

Key Points:

- SoCal urban heatwave activity is increasing at a rapid rate with a greater tendency towards more humid and intense nighttime events
- Heatwaves are persisting later in the year during peak fire season, potentially increasing the intensity of wildfires by enhancing aridity
- Heatwaves have high probability of increasing by 42% in frequency, 26% in duration, and 2°C in temperature during severe drought conditions

Supporting Information:

- Supporting Information S1

Correspondence to:

G. C. Hulley,
glynnc.hulley@jpl.nasa.gov

Citation:

Hulley, G. C., Dousset, B., & Kahn, B. H. (2020). Rising trends in heatwave metrics across Southern California. *Earth's Future*, 8, e2020EF001480. <https://doi.org/10.1029/2020EF001480>

Received 6 JAN 2020

Accepted 4 MAY 2020

Accepted article online 9 MAY 2020

Author Contributions:

Formal analysis: Glynn C. Hulley, Benedicte Dousset, Brian H. Kahn
Funding acquisition: Glynn C. Hulley
Investigation: Glynn C. Hulley
Methodology: Glynn C. Hulley
Software: Glynn C. Hulley
Supervision: Glynn C. Hulley
Writing - original draft: Glynn C. Hulley, Benedicte Dousset
Writing - review & editing: Glynn C. Hulley, Benedicte Dousset, Brian H. Kahn

©2020. The Authors.

This is an open access article under the terms of the Creative Commons Attribution License, which permits use, distribution and reproduction in any medium, provided the original work is properly cited.

Rising Trends in Heatwave Metrics Across Southern California



Glynn C. Hulley¹ , Benedicte Dousset² , and Brian H. Kahn¹ 

¹Jet Propulsion Laboratory, California Institute of Technology, Pasadena, CA, USA, ²Hawai'i Institute of Geophysics and Planetology, University of Hawai'i at Mānoa, Honolulu, HI, USA

Abstract Research on heatwaves has gained significant impetus over the past decade due to a warming planet and rapid 21st century urbanization. This study examines driving factors influencing heatwave trends and interannual variability across Southern California (SoCal) from 1950–2020. Inland urban areas of Los Angeles county are the most susceptible to heatwaves with strong increasing trends in frequency, duration, and intensity that are closely tied to nighttime warming. Coastal and rural areas are less impacted but show a significant increase in heatwave frequency over the past two decades. Heatwave nighttime temperatures combined with high humidity have been increasing at a rapid rate of ~1°C/decade since the 1980s—elevating heat stress and mortality risk to vulnerable urban communities. The increased nighttime humidity is associated with an anomalous moisture source off the coast of Baja California that has intensified over the past decade and is linked to ocean warming trends and changes in the California current system. Heatwaves are starting earlier and ending later in the year for urban regions. This augments public health risks and sets the stage for more intense fall wildfires by enhancing the drying of fuels. Droughts and heatwaves are strongly linked, particularly in inland urban and rural areas that have a high statistical probability of heatwaves increasing in frequency (42%), duration (26%), and daily mean temperature (2.2%) during severe drought conditions. Better understanding of heatwave climate drivers and underlying physical processes could help with prediction skill, in addition to providing effective data-driven recommendations for mitigation efforts in SoCal's vulnerable urban regions.

Plain Language Summary Heatwaves can have a devastating effect on society, infrastructure, and the environment. This study investigates driving factors associated with urbanization, nighttime warming and humidity, ocean dynamics, and droughts that influence heatwaves in Southern California. We show that inland urban heatwaves are rapidly increasing in frequency, duration, and intensity with a greater tendency toward more humid nighttime events—a trend likely to accelerate through the 21st century and linked to human-induced climate change. Coastal and rural areas are less impacted but show a threefold increase in heatwave frequency over the past two decades. Heatwaves have a high probability of increasing by 42% in frequency and by 26% in duration during severe drought conditions. Heatwaves have significantly intensified over the past two decades. They occur later in the year during peak fire season, exposing densely populated regions to the risks of extreme heat, wildfire, and pollution. A better understanding of heatwave dynamics can improve heatwave predictions and help to develop local adaptation and mitigation strategies in vulnerable communities.

1. Introduction

Research on heatwaves and the urban heat island (UHI) effect have gained significant momentum over the past decade due to global warming and rapid urbanization (IPCC, 2013; United Nations, 2015). By 2050 nearly 66% of the world's population will live in cities, a projected increase of 10% from present day with prevailing urbanization occurring in developing countries of Africa and Asia. Urbanization combined with rising temperatures from anthropogenic climate change are projected to significantly warm U.S. cities (Krayenhoff et al., 2018), increasing the probability of extreme heat events (Trenberth et al., 2015) and associated risks of human exposure to deadly heat conditions (Mora et al., 2017).

The frequency, duration, and intensity of heatwaves have increased in several U.S. cities (Habeeb et al., 2015; Shiva et al., 2019) and globally (Perkins et al., 2012), with trends projected to persist in the second half of the 21st century (Gershunov & Guirguis, 2012; Meehl & Tebaldi, 2004; Tebaldi et al., 2006). In general,

heatwaves result from either large-scale upper-level high-pressure systems (“blocking highs”), or synoptic scale ridging that generates warm and dry descending air and corresponding compressional heating that raise air temperatures above normal levels. Blocking highs are responsible for most extreme heatwaves such as those that hit Chicago in 1995 (Meehl & Tebaldi, 2004), Western Europe in 2003 (Black et al., 2004), and Eastern Europe and Russia in 2010 (Matsueda, 2011; Trenberth & Fasullo, 2012).

The detrimental effects of heatwaves are well documented. Heatwaves reduce air quality, dramatically increase electric demand and water usage, and elevate the risks of human morbidity and mortality (Akbari, 2002; Akbari et al., 2001; Anderson & Bell, 2011; Merte, 2017; Son et al., 2012; Tan et al., 2010). In addition to heatwaves, compound events, which are defined as multiday periods of excessive heat following short breaks in heatwave duration, are expected to constitute greater hazards than heatwaves alone under future global warming scenarios (Baldwin et al., 2019). Extreme heat conditions also impact the transportation sector. For example, in 2017 Phoenix Sky Harbor Airport canceled dozens of flights as temperatures reached 49°C—exceeding the operating limitations of smaller regional jets (48°C). In terms of mortality, extreme heat in the United States (U.S.) has resulted in more deaths annually over the past 30 years (136 deaths, compared to 69 for tornadoes and 46 for hurricanes) than all other forms of severe weather (CDC, 2013; NHS, 2016). Nevertheless, heatwaves do not get as much attention in the media, likely because they are not as spectacular and visually appealing as hurricanes and tornadoes, and mainly affect the more marginalized and vulnerable members of society such as the elderly, poor, and disabled (McGeehin & Mirabelli, 2001; Semenza et al., 1996).

While rising heatwave trends are a global issue, they are best demonstrated at the regional scale given the complex atmosphere, ocean, and land interactions driving heatwaves in different regions. In that regard, Southern California (SoCal) is an especially relevant case study given its unique climate and topography dynamics. The SoCal region is home to almost 24 million people, most of whom live in urban areas of greater Los Angeles (L.A.) county (~10 million). This densely populated region is characterized by complex topography and coastal influences resulting in distinct microclimates and ecological zones in which communities are disproportionately impacted by extreme heat events (Hulley et al., 2019). Atmospheric circulation anomalies responsible for most extreme California heatwaves have similar patterns. They feature a strong high-pressure system over the Pacific Northwest that creates a strong surface pressure gradient between a high-pressure anomaly over the Great Plains and a low-pressure system off the coast of southwest L.A. (Gershunov et al., 2009). Transient high-pressure systems in the spring, late summer, or fall are often associated with an offshore flow that draws in dry air from the desert region that gets adiabatically compressed as it flows into the coastal basin producing coastal heatwaves (Clemesha et al., 2018; Gershunov & Guirguis, 2012). Large and persistent blocking high-pressure systems that are more common in summer are frequently associated with a marine layer of varying depth and cooler ocean breezes that are modulated by the intensity and geographical position of the blocking high. These heatwave patterns are frequently associated with more moderate temperatures on the coast and more intense temperatures inland (Gershunov & Guirguis, 2012).

Heatwave metrics such as frequency, duration, intensity, and seasonality/timing can significantly impact public health. Persistent heatwaves with high nocturnal temperatures and humidity limit the ability of people with impaired thermoregulation capacity or chronic illness (particularly the elderly) to recover overnight from the daytime heat stress, resulting in excess mortality rates (Anderson & Bell, 2011; Hajat & Haines, 2002). Gershunov and Guirguis (2012) analyzed current and projected heatwaves over California and found that humid nighttime heatwaves are more affected by climate change than dry daytime heatwaves, although both types are projected to increase, which potentially leads to human heat stress and mortality. For example, in August 2003, the Paris metropolitan area experienced nine consecutive hot days and warm nights that caused 4,867 excess deaths with the highest mortality ratios matching the spatial distribution of nighttime temperatures (Dousset et al., 2011). In areas like L.A., the timing of heatwaves can exacerbate wildfire behavior (Williams et al., 2019), particularly in the fall when extreme temperatures are combined with strong offshore Santa Ana winds that enhance the drying out of fuels and increase the likelihood of fires fully developing after ignition events (Jin et al., 2014; Moritz et al., 2010).

We investigated driving factors influencing the interannual variability and trends in heatwave metrics across urban and rural regions of SoCal from 1950–2020. In section 2 we describe the observational data and

methodologies used for detecting heatwave events. In section 3 we describe and quantify results in terms of heatwave time series and trends, seasonality, increasing humidity, oceanic influences, teleconnections, and drought severity; before summarizing with concluding remarks in section 4.

2. Background and Methodology

2.1. Study Area

The SoCal development pattern is characterized by a high degree of urbanization and low-density population due to the prevalence of single-family detached houses, which are served by decentralized retail areas that rely on complex road networks. Most urban stations lie within the Santa Barbara, L.A., San Bernardino, and San Diego counties within residential areas, airports, and some industrial areas. Rural stations are located in San Diego and Riverside counties and also along the SoCal transverse ranges consisting of mountains and relatively dry valley areas with elevations between 400 and 1,150 m. These stations are usually out of reach of the marine boundary layer being either above it or too far away from it. The predominant vegetation types consist of ponderosa pines and chaparral or shrubs.

2.2. Temperature Data Records

Ground station minimum and maximum surface air temperature data (T_{\min} and T_{\max}) were used to detect and quantify heatwave events from 1950–2020. Data were acquired from the National Climate Data Center's (NCDC) National Weather Service (NWS) Cooperative Observer Program (COOP) (Menne et al., 2012). Station data were not adjusted for any inhomogeneities or urban heat island effects. A subset of stations were selected over SoCal in three distinct subregions: coastal urban, inland urban, and rural (Figure 1). To distinguish urban from rural sites, we used the U.S. Census Bureau maps and land use classification. To qualify as urban, the surrounding area must comprise ~2,500 people, of which at least 1,500 must reside outside institutional group quarters (e.g., nursing homes, hospice, and correctional facilities). Coastal sites are located within 10 km of the ocean. We selected stations with less than 5% of missing data over the entire study period and excluded any years with more than 30 days of consecutive missing data. Missing data were filled by taking an average from neighboring days using a constraint that required no more than two consecutive days missing. If this criterion was not met, values from the closest surrounding station(s) were substituted. Data from stations falling within each subregion were then combined and averaged in the analysis. Given the small amount of missing data from the selected stations and their dense network in SoCal, these interpolations are not expected to introduce any significant bias or error in the resulting trend analyses.

2.3. Gridded Data

Temporal and spatial trends in specific humidity (QV) and total precipitable water vapor (PWV) estimates were investigated using gridded Modern Era Reanalysis for Research and Applications Version 2 (MERRA-2) water vapor fields from 1982–2020 (Gelaro et al., 2017). Daily averaged PWV and QV from MERRA-2 data were estimated from $0.5^{\circ} \times 0.625^{\circ}$ spatial resolution grids at 6-hourly time steps.

We investigated links between sea surface temperatures (SSTs), the California Current System (CCS), and heatwaves in SoCal by calculating SST heatwave anomalies using daily National Oceanic and Atmospheric Administration (NOAA) Optimum Interpolation (OI) V2 high-resolution ($1/4^{\circ}$) gridded SST (Reynolds et al., 2002). The NOAA OI data are constructed by combining observations from various platforms (satellites, ships, buoys) on a regular global grid.

Droughts were quantified using Palmer drought severity index (PDSI) data. PDSI is based on temperature data and the water balance between soil moisture supply and demand through changes in potential evapotranspiration (Palmer, 1965). PDSI data were obtained from the National Center for Atmospheric Research (NCAR) Research Data Archive (RDA) (Dai, 2017) consisting of monthly PDSI over global land areas on a 2.5° grid computed using observed monthly surface air temperature, precipitation, and other surface meteorological forcing data.

2.4. Teleconnection Indices

Trends and correlations between heatwave metrics and the Pacific decadal oscillation (PDO) and El Niño–Southern Oscillation (ENSO) were investigated. Usually, PDO regime shifts occur on multidecadal time steps while ENSO shifts occur approximately every 3–4 years. The warm phase of ENSO (El Niño)

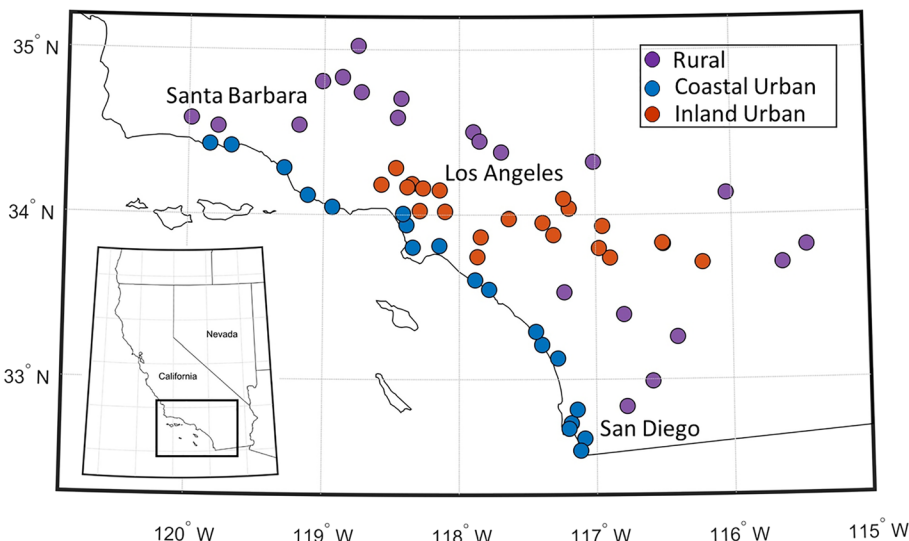


Figure 1. Locations of NCDC COOP stations over Southern California according to three subregions: 21 rural (magenta circles), 19 coastal urban (blue circles), and 20 inland urban (red circles), selected as a function of data reliability and continuity from 1950–2020.

typically contributes to wet winters and warmer temperatures during late summer and fall in the U.S. southwest. Conversely, the cool phase (La Niña) is associated with less precipitation and cooler temperatures in the southwest (Cayan et al., 1999). The PDO index is widely used to monitor decadal variability and record North Pacific SST anomalies (Mantua & Hare, 2002). Positive values are associated with abnormally high SSTs along the North American west coast and below normal SSTs in central/western North Pacific (45°N). Similar to ENSO, PDO influences patterns, frequencies, and magnitudes of precipitation. Its warm phase corresponds to anomalous wet periods in the southwest, but occurs on multidecadal time scales and strongly affects the North American climate (Gershunov & Barnett, 1998; Mantua et al., 1997).

PDO data were acquired from the Joint Institute for the Study of Atmosphere and Ocean (JISAO) (<http://jisao.washington.edu>) (Mantua et al., 1997). To represent ENSO conditions we used the Southern Oscillation Index (SOI) from the Climate Research Unit (CRU) (Ropelewski & Jones, 1987). The SOI is a standardized index based on the observed sea level pressure differences between Tahiti and Darwin (Australia) and coincides with abnormally warm (cold) ocean waters across the eastern tropical Pacific typical of El Niño (La Niña) episodes. Both PDO and SOI data were provided on monthly time steps and for the analysis were averaged to annual time steps for comparison with the regionally averaged heatwave metrics.

2.5. Heatwave Definition and Framework

Currently, there is no universal standard definition of a heatwave. Given a number of consecutive nights/days, a heatwave event is typically estimated from T_{\min} , T_{\max} , or daily average temperatures relative to regional thresholds based on daily and monthly climatological percentiles (Beniston, 2004; Gosling et al., 2007; Gosling et al., 2009; Meehl et al., 2009; Perkins & Alexander, 2013; Robinson, 2001). Heatwave duration is defined as 3 days or more of excess heat above a defined threshold (Collins et al., 2000; Gosling et al., 2007). Some studies have used 6 days (Fischer & Schar, 2010), and a 3-day running window over 5 days (Hajat et al., 2002). Many countries have set their own standards. In the United States the NWS issues an excessive heat warning when the daytime heat index is expected to exceed 40.68°C (105°F) and nighttime minimum temperatures are expected to stay above 26.78°C (75°F) for at least 48 hr. More recently, NWS has introduced an experimental HeatRisk forecast (<https://www.wrh.noaa.gov/wrh/heatrisk/>) consisting of a daily value of expected heat risk for each 24-hr period on a 7-day forecast. Because heatwave patterns differ according to local climate and topography, definitions should include an explicit and separate quantification of daily and nightly temperature extremes (Gershunov et al., 2009). Nighttime high temperatures pose a greater risk to human health because vulnerable people with preexisting conditions such as chronic diseases, or elderly with altered thermoregulation and heat perception are unable to

recover from the high daytime heat and will suffer additional stress from sleep deprivation (Libert et al., 1988). On the other hand, cooler nights during daytime accentuated heatwaves may provide more recovery time and reduce electrical demands and economic burden.

Perkins and Alexander (2013) surveyed a wide range of heat-related indices in the climate science literature and narrowed them down to a set of three robust heatwave definitions that can be calculated from climatological data.

1. The excess heat factor (EHF).
2. CTX90pct. The threshold is the calendar day 90th percentile of Tmax based on a 15-day window centered on a given day; that is, there is a different percentile threshold for each day of the year to account for the seasonal cycle.
3. CTN90pct. The threshold is the calendar day 90th percentile of Tmin instead of Tmax.

The EHF was developed by the South Australian Regional Office (Nairn & Fawcett, 2015) and used extensively to predict heat-related morbidity (IPCC, 2013; Langlois et al., 2013; Nairn & Fawcett, 2015; Wilson et al., 2013). It combines an excess heat index (EHI_{sig}) with an acclimatization index (EHI_{accl}), where EHI_{sig} represents a long-term climate anomaly computed by comparing an average daily temperature over a 3-day period relative to a 95th percentile of daily mean temperature climatology for a reference period, and EHI_{accl} represents the anomaly of the present-day temperatures with respect to the previous 30 days. Including the EHI_{accl} factor considers the heatwave or acclimatization response, but will vary by season and location. For example, smaller anomalies will be found in the tropics compared to the midlatitudes due to differences in the climatic temperature range. Because the units of the EHF are in $^{\circ}\text{C}^2$ it results in a higher signal-to-noise ratio than other definitions. See Text S1 and Figure S1 in the supporting information for a detailed description involving the computation of the EHF and examples of two infamous heatwaves in L.A. during 2006 and 2012.

The CTX90pct and CTN90pct definitions (Alexander et al., 2006; Keggenhoff et al., 2015; Perkins & Alexander, 2013) are based on Tmax and Tmin data, respectively, and account for the seasonal cycle in temperature extremes by employing the 90th percentile thresholds dependent on a 15-day running window for the respective day of year. The percentile value should be chosen to provide statistically relevant measurable events and will not necessarily represent all regions and climate timeframes. For example, Perkins and Alexander (2013) found that a 90th percentile provided a good balance between extreme versus measurable results for their study in Australia. In SoCal, however, we found that a 90th percentile produced extreme results, for example, too many heatwaves that lasted too long. Therefore, we modified the threshold to a 95th percentile that was more consistent with the EHF definition results discussed above and in Text S1. Note that in all text and figures that follow we adjust the notation of CTX90pct as Tmax95 and CTN90pct as Tmin95 for improved readability.

For all three heatwave definitions, we used the World Meteorological Organization (WMO) climate baseline of 1961–1990 to compute the percentile thresholds and detect heatwave events for the period from 1950–2020. Using other baselines (e.g., 1950–1999) somewhat changed the amplitudes of the results but did not affect resulting trends. To fully capture heatwave seasonal trends and statistics we included months in the year from March through November for the detection window. These heatwave events were subsequently characterized using four metrics.

1. Frequency—number of heatwaves per year within detection window.
2. Season length—number of days from first to last heatwave event in any given year.
3. Intensity—maximum temperature during a heatwave event minus the 90th percentile climatology of temperatures for a 15-day window centered on the heatwave event. Note that since the EHF includes an acclimatization factor resulting in units of $^{\circ}\text{C}^2$, the EHF intensity is computed from the excess heat index factor (see Equation S1 in Text S1)—the average daily temperature over a 3-day period relative to a reference 95th percentile.
4. Duration—total number of contiguous days from start to end of heatwave event.

These metrics were averaged for each station within each subregion and their statistics and trends were computed for the 1950–2020 period. These heatwave definitions and metrics are currently recommended by the

Commission for Climatology (CCl) Expert Team on Climate Risk and Sector-specific Climate Indices (ET CRSCI) of the WMO World Climate Programme (Keggenhoff et al., 2015; McGregor et al., 2015). Perkins and Alexander (2013) showed that all three definitions resulted in very similar trends in all heatwave metrics from 1951–2008 in Australia, indicating a level of robustness regardless of the index used. However, that level of agreement is not necessarily true for other areas of the globe due to regional and local variability in climate and surface characteristics. For example, California heatwaves in the 21st century are often expressed as either dry daytime accentuated heatwaves or humid nighttime accentuated heatwaves (Gershunov & Guirguis, 2012). To get a more holistic perspective, we looked at trends using all three heatwave definitions and metrics described above.

3. Results and Discussion

3.1. Heatwave Trend Analysis

Figure 2 shows time series and trends in heatwave metrics (frequency, intensity, duration) for each heatwave definition and SoCal subregion with data averaged over 5-year periods. Trend lines were plotted for each definition only when statistically significant ($p < 5\%$). Table 1 summarizes the regression statistical analysis and uncertainty estimates in decadal (dec) trend values for each definition, metric, and subregion.

All three regions show statistically significant rising heatwave metric trends for at least one heatwave definition with the exception of intensity for the coastal urban and rural areas. Inland urban regions show the strongest trends for all heatwave metrics with R^2 ranging from 0.68–0.84 ($p \ll 1\%$) for EHF/Tmin95 definitions and the only region with rising trends in intensity for all definitions. The Tmin95 definition had the strongest trends for all metrics ($R^2 > 0.7$, $p \ll 1\%$), followed by EHF and Tmax95. For Tmin95, results in Figure 2 and Table 1 show rising trends of 1.4 num/dec in frequency, 0.34 days/dec in duration, 0.18°C/dec in intensity, and 0.84 month/dec in season length between 1950 and 2020. Taking an average of all three heatwave definitions, in the past 5 years inland urban regions have experienced nine heatwaves per year, lasting on average 6 days. For heatwave frequency, the Tmin95 trend (1.4 num/dec) was almost 3 times greater than EHF (0.51 num/dec) and Tmax95 (0.5 num/dec) trends, with values for frequency (12 per year) and duration (7 days) over the past decade. Similar to inland urban, the coastal region had stronger frequency trends for Tmin95 (0.71 num/dec)—more than doubling that of EHF (0.3 num/dec) and Tmax95 (0.33 num/dec). For rural regions the trend values for frequency were similar to the coastal region but with higher values on average (8 per decade presently as opposed to 6 for coastal). The enhanced Tmin95 trends for all regions when compared to other definitions are consistent with a rise in nighttime-accentuated heatwaves since the late 1990s with respect to background mean warming (Gershunov et al., 2009; Gershunov & Guirguis, 2012) and will be discussed in section 3.6 with respect to rising humidity levels.

Heatwave intensity had a positive trend for the inland urban region for all three definitions, with Tmax95 intensities 1.5–2 times higher than Tmin95 and EHF. Similarly, for the coastal region Tmax95 had the highest intensity values between 4°C and 6°C—on average ~3°C higher than the Tmin95 and EHF definitions. This is likely due to larger variance in daytime Tmax temperatures, especially along coastal regions during heatwaves with enhanced offshore flow conditions. The marine boundary layer along the coast also reduces the daytime climatological mean values relative to heatwave maximum temperatures. Rural intensity values were similar in magnitude and variance for all definitions revealing a symmetry in the diurnal cycle between the maximum Tmin/Tmax heatwave temperatures and climatological mean values, and the moderating effect of the surface latent heat fluxes.

A concerning trend for urban regions is a sharp rise in frequency, duration, and season length over the past two decades. For the Tmin95 definition since 2000, frequencies rose from 6 to more than 10 (inland) and from 3 to more than 6 (coastal) per year on average, and season length increased from 5 to 7 months for inland areas and from 3 to 5 months for coastal areas. These recent increases could be associated with changes in cloud dynamics in the region. Recent studies showed that coastal low cloudiness (CLC) is one of the key modulating factors that influences the intensity and timing of coastal heatwaves (Clemesha et al., 2018) because they reflect solar energy back to space and prevent heating of the surface. Furthermore, SoCal coastal areas have experienced a reduction in fog and summer cloud frequency in recent decades due to a combination of anthropogenic and urbanization-induced warming (LaDochy & Witiw, 2012; Williams et al., 2015, 2018). These reductions in cloud shading significantly increase daytime

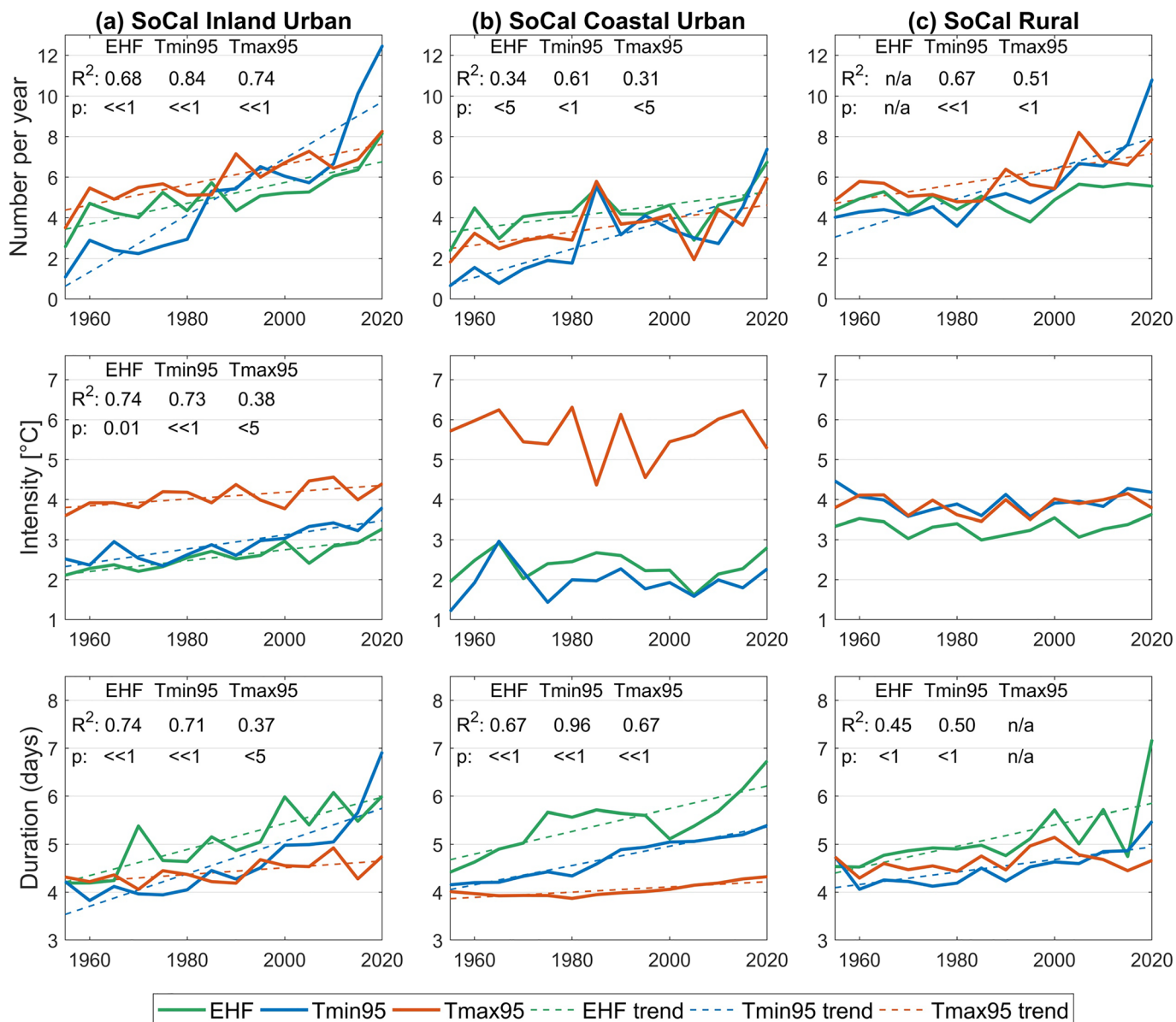


Figure 2. Heatwave time series and trends from 1950–2020 for SoCal (a) inland urban, (b) coastal urban, and (c) rural regions for heatwave severity metrics of frequency (number/year), intensity (°C), and duration (days). Statistically significant ($p < 5\%$) trend lines and stats are shown for the three different heatwave definitions (EHF, Tmin95, Tmax95). Circles and solid error bars show 5-year average values and associated standard deviations. All heatwave definitions use the WMO climate baseline of 1961–1990. Note that since the EHF includes an acclimatization factor resulting in units of °C², the EHF intensity is computed from the excess heat index factor (see Equation S1 in the supporting information)—the average daily temperature over a 3-day period relative to a reference 95th percentile.

solar irradiance and evaporative demand (Williams et al., 2018), resulting in positive cloud-warming feedbacks that increase the probability of both heatwaves and wildfires.

3.2. Heatwave Duration-Intensity Coupling

While the analysis so far has focused on individual heatwave metric trends, studies indicate that a multivariate approach considering all metrics in a more comprehensive manner may better represent the full impact of heatwave events (Mazdiyasni et al., 2019; Ouarda & Charron, 2018). Quantifying the likelihood of heatwave events occurring with different intensities and durations can have practical applications. For example, the optimal design of electrical grids during peak demand must consider both intensity and duration of excessive heat concurrently (Mazdiyasni et al., 2019). We quantified the relationship between heatwave

Table 1

Linear Regression Statistical Analysis of Heatwave Decadal Trends Including Uncertainty for Three Heatwave Definitions and Four Heatwave Metrics From 1950–2020 for the SoCal Inland Urban, Coastal Urban, and Rural Regions Using NCDC Surface Air Temperature

Heatwave definition	Heatwave metric	SoCal inland urban			SoCal coastal urban			SoCal rural		
		Decadal trend	R ²	p (%)	Decadal trend	R ²	p (%)	Decadal trend	R ²	p (%)
EHF	Frequency	0.51 ± 0.20	0.68	<1	0.30 ± 0.25	0.34	2.99	-	-	-
	Duration (days)	0.27 ± 0.09	0.74	<1	0.24 ± 0.10	0.67	<1	0.22 ± 0.14	0.45	0.82
	Intensity (°C)	0.14 ± 0.05	0.74	<1	—	—	—	—	—	—
	Season length (days)	0.25 ± 0.07	0.80	≤1	—	—	—	—	—	—
Tmin95	Frequency	1.4 ± 0.36	0.84	≤1	0.71 ± 0.33	0.61	<5	0.75 ± 0.30	0.67	<1
	Duration (days)	0.34 ± 0.13	0.71	<1	0.20 ± 0.02	0.96	≤1	0.13 ± 0.08	0.50	<5
	Intensity (°C)	0.18 ± 0.06	0.73	<1	—	—	—	—	—	—
	Season length (days)	0.84 ± 0.16	0.91	≤1	0.55 ± 0.26	0.6	<5	0.31 ± 0.15	0.60	<5
Tmax95	Frequency	0.50 ± 0.17	0.74	<1	0.33 ± 0.29	0.31	3.94	0.38 ± 0.21	0.51	<5
	Duration (days)	0.07 ± 0.05	0.37	2.02	0.05 ± 0.02	0.67	<1	—	—	—
	Intensity (°C)	0.09 ± 0.06	0.38	1.90	—	—	—	—	—	—
	Season length (days)	0.21 ± 0.14	0.41	1.37	—	—	—	—	—	—

Note. datafrequency = number detected/year; duration = total consecutive days; intensity = °C; and season length = number of days from start of first heatwave to end of last heatwave detected for any particular year. Error estimates in the trends are calculated in the standard way as SE = sqrt[cov (var(R))], where R = regression residuals.

duration and intensity to better understand their synergy, magnitudes, and variability for different time periods.

Figure 3 shows boxplots of heatwave duration versus intensity for the three regions by averaging all heatwave data for the three definitions over the study period. In addition, we show how this relationship changes for two different time periods (1950–1990 and 1990–2020). The strongest coupling between duration-intensity occurs for inland urban and rural regions, while for coastal areas it is much weaker. For example, the most intense heatwaves (>6°C) last on average 10 days for inland urban, but 6 days for coastal urban, likely due to Santa Ana wind offshore flow conditions (Guzman-Morales et al., 2016). When looking at coupling differences for two different time periods (1950–1990 vs. 1990–2020) we see that the duration-intensity relationship strengthens with increasing intensity for inland urban during the 1990–2020 period, that is, above ~3°C intensity, heatwaves with similar intensity are lasting longer. For coastal urban this change is more uniform across intensities with heatwaves lasting between 2 and 3 days longer irrespective of intensity. This could be the result of the weaker upwelling during the summer months in recent decades (Brady et al., 2017) that decreases the ocean-land temperature gradients and subsequently reduces sea breezes and cooling. For rural areas we see a pronounced increase in duration versus intensity for the 1990–2020 regime, possibly associated with the intense drought in California between 2012–2016.

3.3. Heatwave Seasonality

We further investigated the seasonality and timing of heatwaves that can have significant societal impacts. For example, heatwaves earlier in the year pose a greater risk to human health than heatwaves of the same magnitude occurring later in the year (Guirguis et al., 2014, 2018). This is because in early spring people are not yet acclimated to high temperatures and are more vulnerable to heat stress (Habib et al., 2015; Hajat & Haines, 2002; Kalkstein & Greene, 1997). Heatwaves persisting later in the year in the SoCal region have the potential to be associated with increased wildfire risk by further drying out fuels and enhancing aridity, particularly if they coincide with strong offshore Santa Ana wind conditions at the end of the dry season (Jin et al., 2014; Williams et al., 2019). For example, the Thomas fire in December 2017 and the Woolsey fire in November 2018, which caused tremendous devastation in Ventura, Santa Barbara, L.A., and San Bernardino counties were both preceded by record-breaking heatwaves during the late summertime. In the Fall, California wildfires are driven by complex convergent processes, including the following: already dry fuels after summer, Santa Ana wind conditions, a late onset of cold-season precipitation, fuel abundance, and human-caused ignition (Williams et al., 2019). All else being equal, more intense and frequent fall heatwaves should increase wildfire danger, particularly when coinciding with Santa Ana wind conditions. However, there are other factors at play and while large fall wildfires have become more frequent in California over the past several decades in the North Coast and Sierra Nevada regions, there have been no

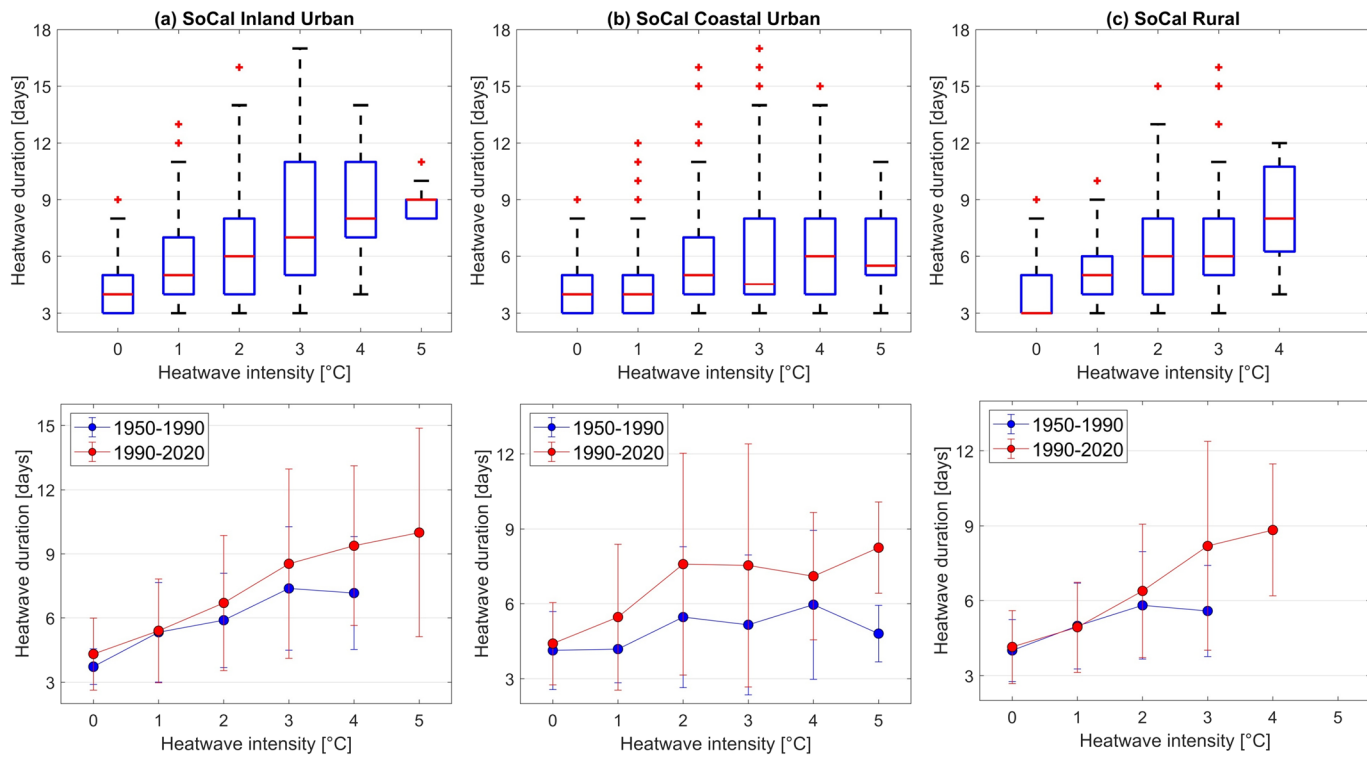


Figure 3. (top row) Boxplots of heatwave duration-intensity relationships, and (bottom row) duration-intensity relationships shown as error bars for two different time periods (1950–1990 and 1990–2020), for SoCal (a) inland urban, (b) coastal urban, and (c) rural regions.

increases in SoCal coastal or inland urban burned area or wildfire frequency in recent decades (Williams et al., 2019). Possible reasons for this that deserve further study are as follows: more precautionary measures being taken against accidental ignitions, increased population available to put out fires, vegetation type transitions in some area areas (Keeley et al., 2005), and increased fragmentation of natural landscapes with urban expansion reducing connectivity of burnable wildlands (Balch et al., 2017; Keeley & Syphard, 2018).

We looked at trends in three seasonality metrics: season length, defined as the number of decimal months from the first heatwave detected in the year to the last; month of first heatwave detected; and month of last heatwave detected. Results in Figure 4 and Table 1 show that heatwave season length for Tmin95 increased at rates of 0.84, 0.55, and 0.31 months/dec since 1950 for inland, coastal urban, and rural areas, respectively. The EHF definition in general had much lower season lengths than either Tmin95 or Tmax95 likely because of the acclimatization term that acts as a dampening factor with respect to seasonal change and also because the climatology reference is computed for the entire year (while Tmin95/Tmax95 definitions use present 15-day windows). Are these rising trends due to heatwaves starting sooner or ending later in the year, or a combination of the two? In terms of timing, Figure 4 results for Tmin95/Tmax95 show that heatwaves in present day are starting earlier in the year in late March for all three regions, as opposed to starting in April–May in the 1950s. For example, an early spring heatwave in SoCal in late April 2014 set record daytime temperatures of 28–32°C along the coast, and 32–36°C inland. For the EHF this trend was weaker but still showed an earlier start of 0.42 months for inland and coastal urban. Only the inland urban region showed an increasing trend in month of last heatwave detected with a rate of 0.27 months/dec for the Tmin95 definition and 0.11 months/dec for EHF, with heatwaves that used to end in August now ending in late September, on average for both definitions.

3.4. Rising Heatwave Nighttime Temperatures and Humidity

A study of heatwaves from 1948–2006 ending with the July 2006 extreme heat event over California and Nevada (Gershunov et al., 2009) showed an increasing trend in more humid nighttime temperatures in California. This was attributed to an anomalous moisture source over a marine region off the west coast

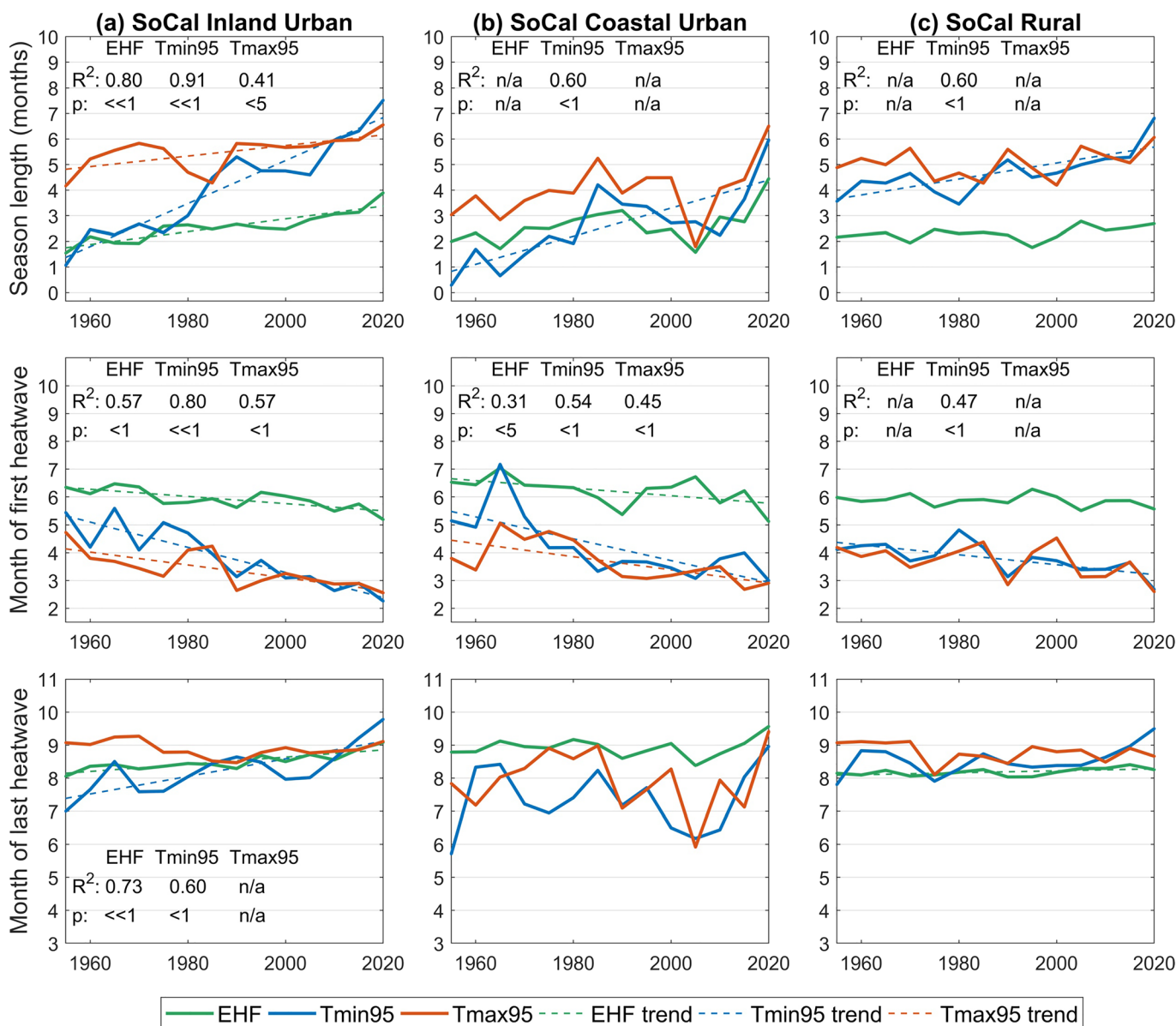


Figure 4. Time series in heatwave seasonality from 1950–2020 showing from top to bottom; season length (months), month of first heatwave in year, and month of last heatwave in year for all three heatwave definitions in SoCal (a) inland urban, (b) coastal urban, and (c) rural regions. Trends are plotted only if statistically significant ($p < 5\%$).

of Baja California coinciding with a warming SST trend in the region associated with anthropogenic climate change (Barnett et al., 2001; Barnett et al., 2005; Pierce et al., 2006). This moisture source combined with a synoptic circulation pattern advected moisture into the U.S. southwest increasing the frequency and intensity of nighttime heatwaves.

We investigated the persistence of this anomalous moisture source and quantified its effect on increasing nighttime heatwave temperatures in the SoCal region over the past two decades. We first looked at trends in MERRA-2 QV and total PWV estimates over the western and southwestern U.S. from 1982–2020. Figure 5 shows the MERRA-2 PWV and QV anomalies (700 hPa, 850 hPa) represented as the difference between daily average values during heatwave dates and the average summer (JJA) climatology from 1982–2020. Wind anomaly vectors (heatwave minus JJA) derived from the MERRA-2 data are overlaid on the QV images. The results in Figure 5a reveal a strong moisture anomaly in excess of 10 mm in PWV off the northwest coast of Baja California (30°N , 116°W), which extends over land into northern Baja and the

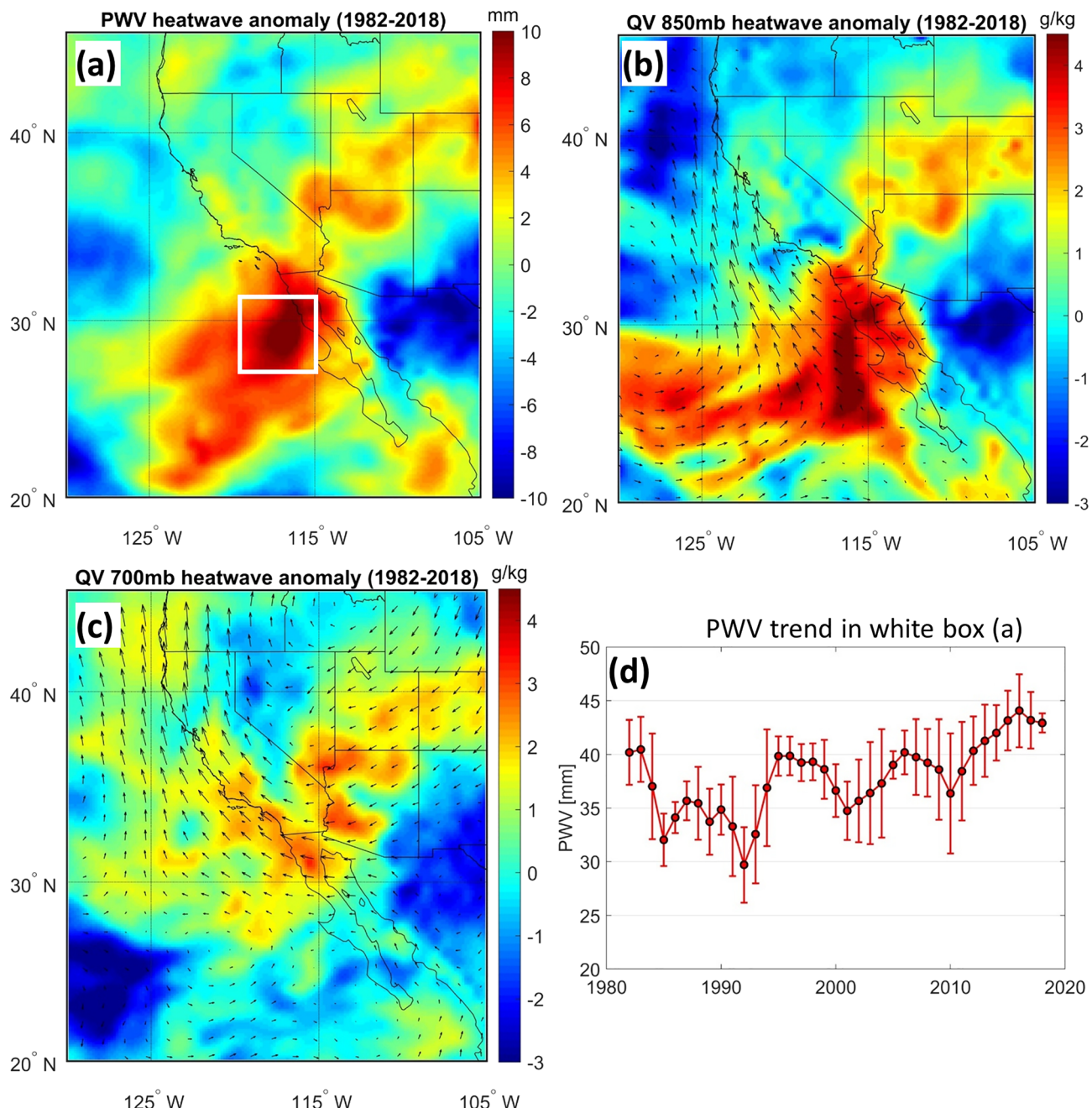


Figure 5. MERRA-2 heatwave moisture anomalies from 1982–2020 (heatwave events minus JJA summer climatology) for (a) precipitable water vapor (PWV); (b) 850 hPa specific humidity (QV) with 850 hPa wind anomaly plotted as arrows; (c) 700 hPa specific humidity (QV) with 500 hPa wind anomaly; and (d) average PWV trend for box shown in (a).

SoCal region and appears to have strengthened with PWV values increasing by ~20% from ~35 mm in 2000 to almost 45 mm in 2018 (Figure 5d).

This moistening trend has coincided with a persistent continental atmospheric high-pressure system in proximity to a low-pressure system off the California coast. The resulting pressure gradient leads to a reduction in the typical northwesterly flow, occasionally reversing into a south-southeast (SSE) flow. This flow pattern is evident by the wind anomaly vectors predominately from the SSE direction in Figures 5b and 5c. The absence of anomalies at 850 hPa over land are probably due to topography effects at those levels. This change in circulation is likely responsible for moist air flowing into the northern Baja and the SoCal

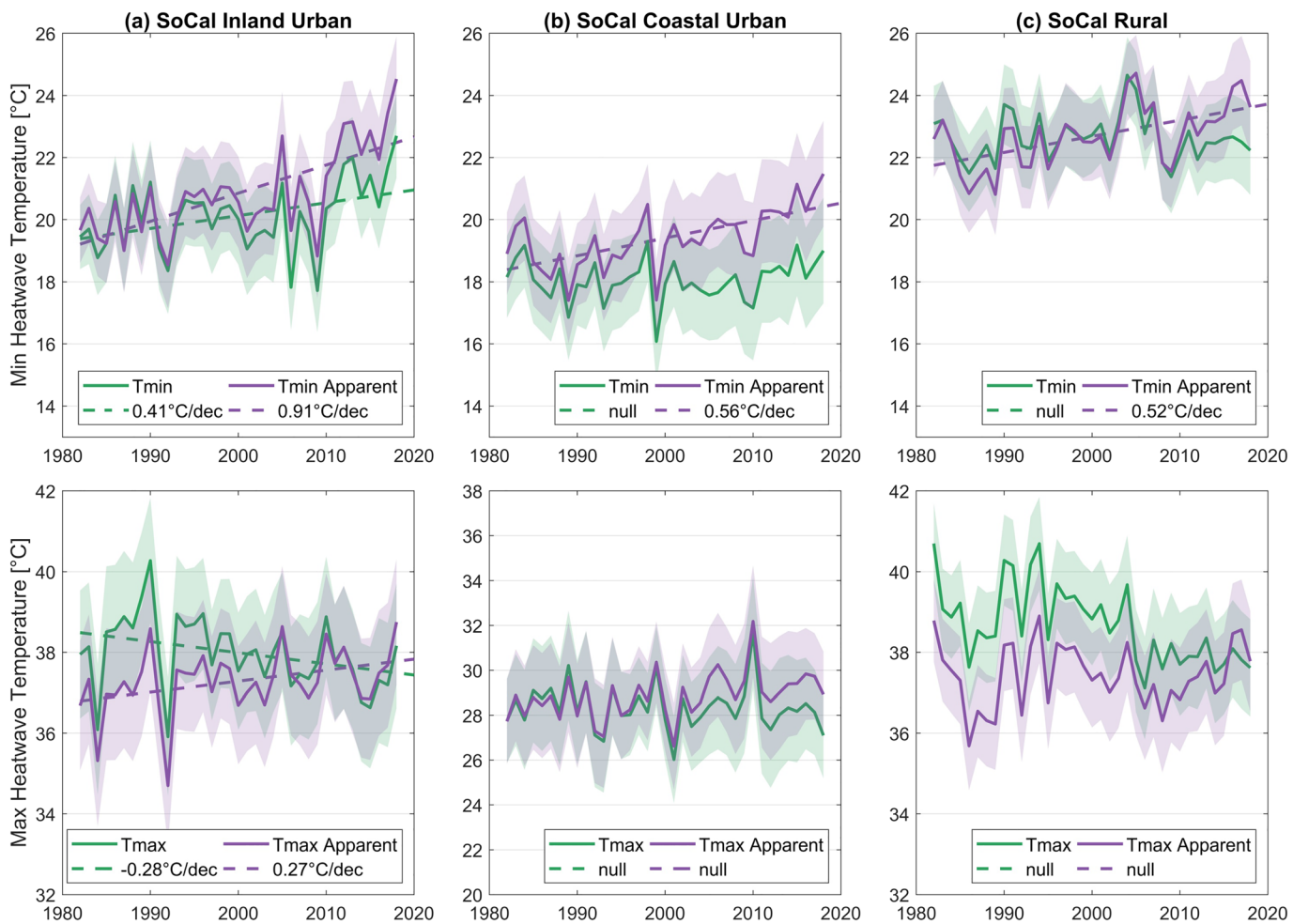


Figure 6. Mean annual time series of heatwave ambient and apparent Tmin (top panels), and ambient and apparent Tmax (bottom panels) computed by combining ground station air temperature with relative humidity fields from MERRA-2 from 1982–2020 for SoCal (a) inland, (b) coastal urban, and (c) rural sub regions. Solid error bars represent the annual standard deviation. Only trends with p values of $<5\%$ are shown.

region during heatwave events. Figure 5b shows that QV anomalies can reach up to 5 g/kg at 850 hPa over a broad area consistent with the peak PWV anomaly region off the coast of Baja, while anomalies at 700 hPa in Figure 5c reach near 3 g/kg but are constrained mostly to coastal regions of SoCal and northern Baja. QV anomalies in the free troposphere above 800 hPa have a much larger greenhouse effect than equivalent anomalies located in the boundary layer and are responsible for ~90% of the water vapor feedback (Soden et al., 2008). QV anomalies further impact stratocumulus height, base, and liquid water path (Christensen et al., 2013), although the impacts of free tropospheric anomalies on marine boundary layer structure in heatwaves are unclear and deserve further study.

To better quantify this effect, we looked at trends in ambient and apparent heatwave Tmin and Tmax temperatures. Ambient temperature refers to the air temperature of the immediate surroundings, while apparent temperature considers the effects of humidity and represents the physiological impact of temperature on the human body due to decreased efficacy in perspiration evaporation. Ignoring the effects of wind and solar radiation, the apparent temperature, $T_{i,a}$, can be calculated as follows: $T_{i,a} = -1.3 + 0.92T_i + 2.2e$, where T_i is ambient air temperature ($^{\circ}\text{C}$) and e is water vapor pressure (kPa) as an indicator of humidity (Steadman, 1984). Surface water vapor pressure was estimated from the 2 m MERRA-2 specific humidity (Q2m) using standardized formulations for saturation vapor pressure and grid boxes corresponding to nearest station locations for the three subregions of the study.

Figure 6 shows the mean annual time series of heatwave ambient and apparent Tmin and Tmax and their associated trends using heatwaves detected from all three definitions to avoid any biases. Since

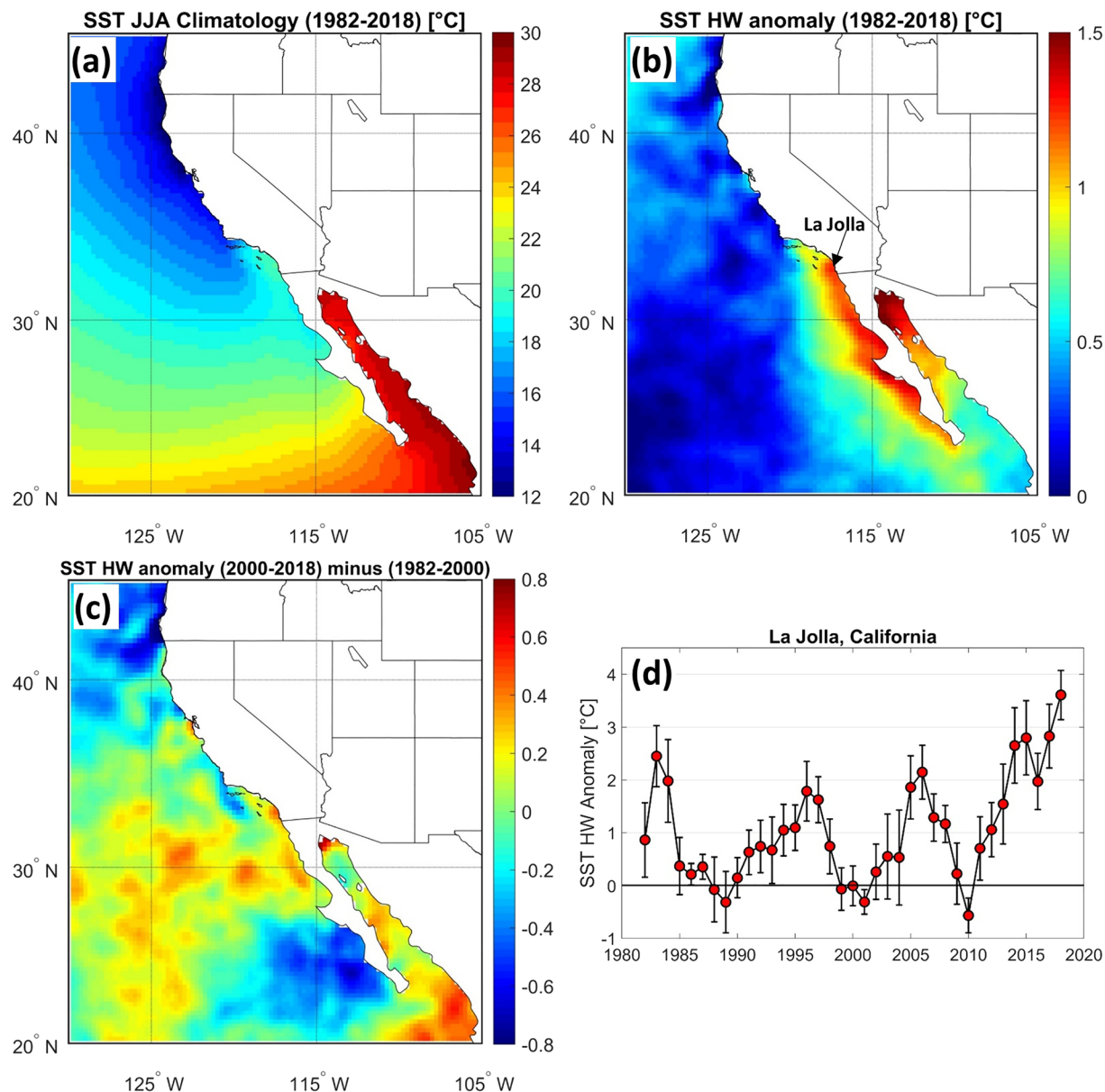


Figure 7. (a) SST June–July–Aug (JJA) climatology. (b) SST heatwave (HW) anomaly map of average SST during SoCal land heatwaves and SST JJA climatology between 1982 and 2020. (c) Difference between the SST heatwave anomaly between two 20-year periods (2000–2020 and 1982–2000). (d) SST heatwave anomaly time series between 1982 and 2020 off the coast of La Jolla, California indicated in (b).

1980 inland urban regions showed positive trends for both Tmin temperatures but only for apparent Tmax temperatures. Apparent Tmin trends ($0.91^{\circ}\text{C}/\text{dec}$) almost double the ambient Tmin trends ($0.41^{\circ}\text{C}/\text{dec}$), while the apparent Tmax trend ($0.27^{\circ}\text{C}/\text{dec}$) contrasts with a negative ambient Tmax trend ($-0.29^{\circ}\text{C}/\text{dec}$), indicating a strong influence of rising humidity levels on both day and nighttime ambient temperatures. For coastal urban only apparent Tmin had a significant trend ($0.56^{\circ}\text{C}/\text{dec}$). Similarly, rural regions showed an increasing trend in apparent Tmin of $0.52^{\circ}\text{C}/\text{dec}$ with no trends in Tmax temperatures.

The observed rising trends in ambient Tmin for inland urban areas alone would not be complete without a discussion on the effects of urbanization on Tmin. Urbanization alters the partition of the surface energy budget by shifting the balance from latent to sensible heat fluxes. In particular at nighttime, urban areas gradually reradiate the heat stored during the day causing a surface warming forcing, while rural areas cool off faster due to reduced heat capacities and unobstructed outgoing radiation (higher sky

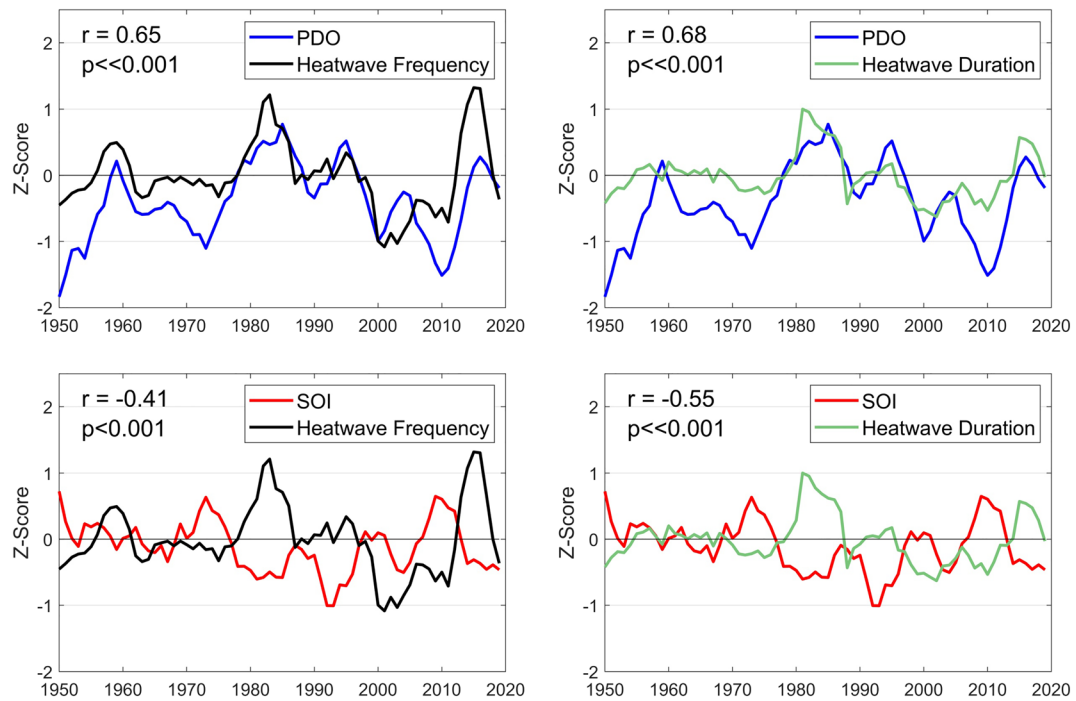


Figure 8. Time series of annual average EHF heatwave frequency and duration versus PDO and ENSO (SOI) for the SoCal coastal urban region from 1950–2020. Heatwave frequency and duration were detrended by removing residuals from the regression line and their z scores calculated to allow a one-to-one comparison with PDO/ENSO data.

view factor), resulting in a cooling forcing. This contrast generates the UHI effect (Dousset & Gourmelon, 2003; Grimmond & Oke, 1999; Luval et al., 2015). In L.A., for example, nighttime temperature differences of 2°C or more between inland urban and coastal urban areas, and a UHI of 5°C between downtown L.A. and rural areas are typical (Dousset & Gourmelon, 2003; Taha, 2015). There is a much stronger correlation between the effects of urbanization (represented by population growth in LA county) on Tmin for urban areas when compared to rural areas since the 1940s. This is further discussed in Text S2 and illustrated in Figure S5. Interannual variation between annual average Tmin and heatwave frequencies also are closely linked with r values ranging from 0.57–0.83 for all regions as shown in Figure S6.

3.5. Oceanic Influence

Observations have shown that anthropogenic forcing has in general warmed the ocean surface with regional variations over the last 40 years (Pierce et al., 2006). This has coincided with the recent emergence of anthropogenic trends in the California Current System (CCS) resulting in intensification of cold upwellings in spring with reductions in subsequent summer months (Brady et al., 2017). These CCS variations have further coincided with a significant increase in marine heatwaves over the past century (Oliver et al., 2018). To better understand the links between SSTs, CCS, and heatwaves in SoCal, we calculated a SST heatwave anomaly from 1982–2020 using daily NOAA OI V2 high-resolution (1/4°) gridded SST (Reynolds et al., 2002). Here we define a SST heatwave as the difference between average SSTs calculated during heatwave events, and an average summertime (JJA) SST climatology shown in Figure 7a. The SST heatwave map in Figure 7b shows a significant ocean warming of up to 1.5°C that extends from Baja California up to the SoCal Santa Barbara county. The warming anomaly encompasses most of the Gulf of California and extends to ~300 km offshore from SoCal and the Baja California coastline. It is consistent with a warming SST trend in the same region from 1945–2004 (Pierce et al., 2006) and part of an ocean surface warming pattern linked to an increase in net surface heat flux from anthropogenic climate change (Barnett et al., 2001, 2005). The anomalous differences between two ~20-year periods (1982–2000 and 2000–2020) in Figure 7c show that over the past two decades the warming trend has intensified up to 0.8°C over large regions off the coast of

Table 2

Summary of Correlations Between PDO, SOI for Four Heatwave Metrics (Frequency, Length, Tmin, and Tmax) Over the Inland Urban, Coastal Urban, and Rural Regions From 1950–2020

Region	Climate signal	Frequency	Duration	Tmin	Tmax
Coastal urban	PDO	0.65 (0.0)	0.68 (0.0)	0.52 (0.0)	—
	SOI	-0.41 (0.0)	-0.55 (0.0)	-0.26 (2.9)	—
Inland urban	PDO	0.41 (0.0)	—	—	—
	SOI	—	-0.30 (1.3)	—	—
Rural	PDO	—	—	-0.31 (0.8)	—
	SOI	—	—	—	—

Note. Results of the bivariate correlation are shown by r values, with corresponding p values (%) in parentheses. Only values at the <5% significance level are shown.

northern Baja and SoCal. For example, SST anomalies off the coast of La Jolla have exceeded 3°C for the first time in the 1980–2020 record (Figure 7d) and continue to rise.

Interestingly, the warming over the ocean centered at 30°N, 125°W coincides in space and time with the persistent moisture anomaly (Figure 5). Synoptic circulation patterns over the past few decades associated with warmer SSTs have resulted in mean surface winds blowing predominately from the south, southeast (downwelling favorable winds). Over the last decade, this pattern has reduced upwellings in summer months and sustained a cap of warmer ocean waters from southern Baja to the coast of Santa Barbara. A good example is the extreme heatwave that affected SoCal area in July 2006 when an influx of monsoonal moisture from Baja California resulted in maximum transport of moisture over southern California (Gershunov et al., 2009; Kozlowski & Edwards, 2007).

The positive feedback between unusually high nighttime temperatures and humidity (Gershunov et al., 2009) resulted in a mortality of around 600 deaths with 131 from hyperthermia alone (Guirguis et al., 2014; Ostro et al., 2009), putting a severe strain on California's economy and energy supply (Knowlton et al., 2009).

3.6. Teleconnections

We investigated trends and correlations between heatwave metrics and PDO and ENSO (represented by SOI). Figure 8 shows detrended time series of heatwave frequency and duration versus PDO and ENSO for the coastal urban subregion from 1950–2020 (see Figure S3 for inland urban). Heatwave metrics were detrended by removing residuals from the regression line and their z scores calculated to allow a one-to-one comparison with PDO/ENSO data. Since 1950 we observe three complete cycles of the PDO with modulations predominately in the cold phase. There are two cold phases from 1943–1979 and 1998–2017, and a warm phase from 1979 through the late 1990s. Table 2 shows Pearson's bivariate correlations between the EHF heatwave metrics and PDO/ENSO and only reported if statistically significant ($p < 5\%$). For coastal urban areas, PDO has a strong positive relationship between heatwave frequency ($r = 0.65$), duration ($r = 0.68$), and Tmin ($r = 0.52$), and no correlation with heatwave Tmax. Therefore, warm phases of the PDO explain a large proportion of variance associated with heatwave activity along the coast, however, this relationship weakens further inland for the urban inland and rural sub-regions, with only inland showing a

positive correlation with PDO and heatwave frequency ($r = 0.41$, see Figure S3). For ENSO, the relationships for coastal urban are slightly weaker and more variable, with negative correlations for both frequency ($r = -0.41$) and duration ($r = -0.55$). Temperature relationships were much weaker with only Tmin being statistically significant ($r = -0.26$). This indicates that atmospheric circulation patterns during positive ENSO are likely correlated with less heatwave activity in terms of frequency and duration and vice versa.

Studies show that in-phase modulations of PDO and ENSO result in a stronger ENSO climate signal with regard to winter precipitation in the western United States, while out-of-phase relationships have a weaker climate signal (Gershunov & Barnett, 1998). We looked at statistics of heatwave metrics for all six possible PDO/ENSO regimes. While the results in Figure S4 showed no clear distinction between different ENSO modulations associated with each PDO phase, the +PDO/N (warm PDO, neutral ENSO) had the largest proportion in terms of heatwave frequency on average (20%). Other work has shown that decades of cold PDO in combination with dry signals associated with years of neutral ENSO and La Niña are more prone to drought conditions in the U.S. southwest (Goodrich, 2007). While results in the next section show an increased probability of heatwaves during severe droughts (but not mild to

Table 3

Results of Paired-Sample t Test of Probability Distributions of Different Drought Severities (Mild–Moderate vs. Severe) for Three Heatwave Metrics (Frequency, Length, Daily Mean Temperature [DMT]) Over the Inland Urban, Coastal Urban, and Rural Regions From 1950–2020

Heatwave metric	Mild–moderate vs. severe drought		
	<i>h</i>	<i>p</i>	<i>tstat</i>
Inland urban	Frequency	1	0.010
	Length	1	0.021
	DMT	1	0.016
Coastal urban	Frequency	0	0.418
	Length	1	0.027
	DMT	0	0.075
Rural	Frequency	0	0.080
	Length	0	0.230
	DMT	0	0.960
			-0.11
			-0.11
			-0.16
			-0.26
			-0.62

Note. The decision value (h) indicates if the t test rejects the null hypothesis ($h = 1$) at the 5% significance level, given by p , while $tstat$ is the value of the test statistic, where the greater the magnitude of $tstat$, the greater the evidence against the null hypothesis. Only values in bold are significant at the 5% level.

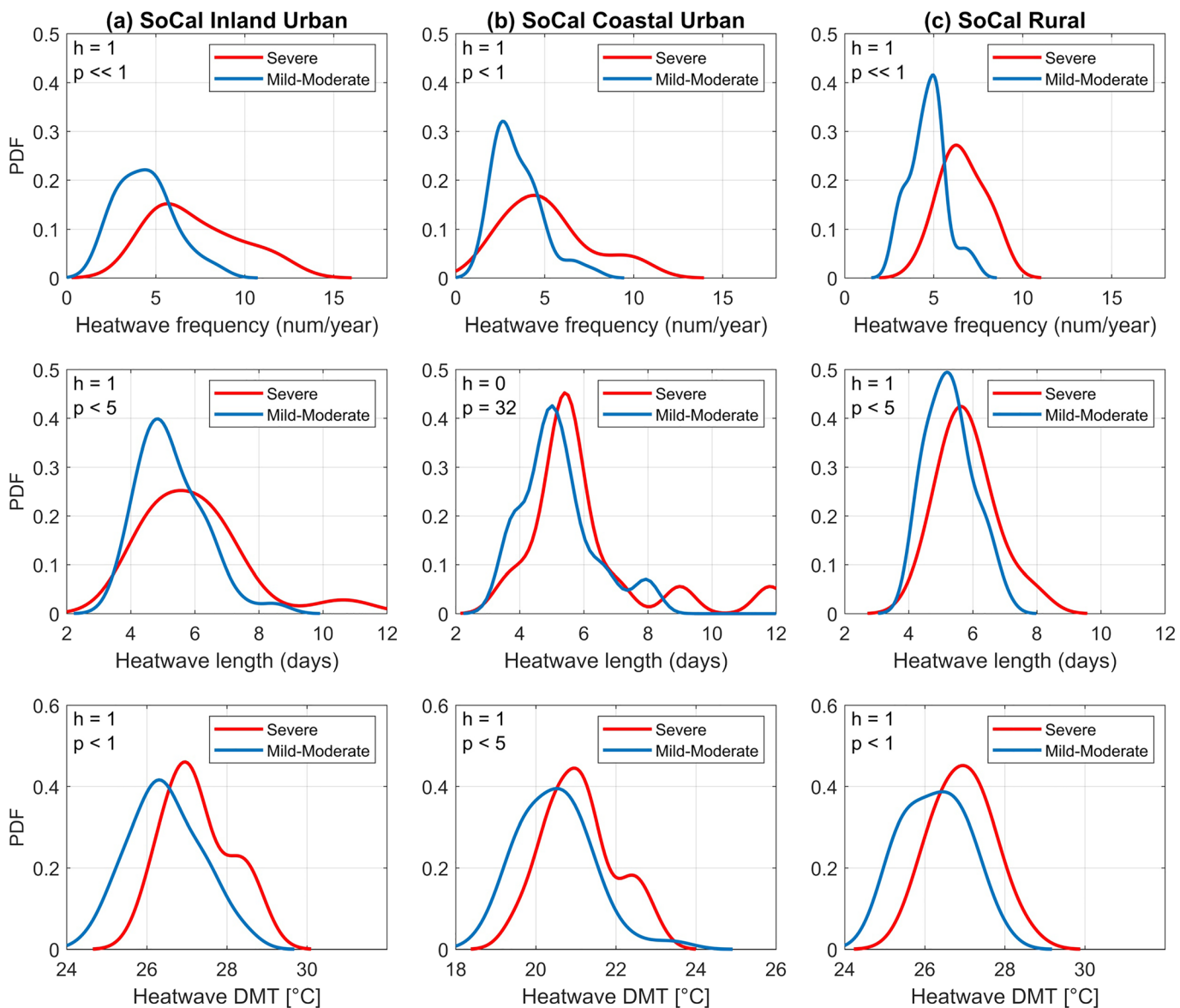


Figure 9. Probability density functions (PDFs) for mild to moderate drought (blue), and severe drought (red) versus heatwave frequency, length, and daily mean temperature (DMT) for SoCal (a) inland urban, (b) coastal urban, and (c) rural regions.

moderate ones), the above results indicate higher heatwave activity in terms of frequency and duration during warm phases of the PDO, irrespective of ENSO phase. In fact Alfaro et al., (2004) showed that high summertime temperatures in general along the California coast are correlated and may be predicted from warm springtime phases of the PDO.

3.7. Drought Severity

Droughts, like heatwaves, have captured the world's attention in recent decades due to their costly and deadly impacts. Some examples include the following: the extreme California drought from 2012–2016 that resulted in substantial groundwater depletion and a state of emergency; Australia's "Millennium" drought from 1995–2009 that resulted in billions of dollars spent on desalination plants; and the Cape Town drought from 2015–2018 resulting in the "Day Zero" scenario. Due to global warming, droughts occur more quickly with greater intensity and persistence because higher temperatures lead to greater evaporation and surface drying (Lau & Kim, 2012; Trenberth, 2011). In Mediterranean climate regions, drought is also due to a longer dry season, as the subtropical belt extends poleward (Polade et al., 2017).

Droughts in California primarily arise from a lack of winter precipitation such as the most recent 2012–2016 extreme drought (AghaKouchak et al., 2014; Cheng et al., 2016; Mao et al., 2015). California's most significant historical statewide droughts were those of 1929–1934, 1976–1977, 1987–1992, and 2012–2016, all with severe hydrologic impacts (Jones, 2015; Swain et al., 2014). Recent climate studies revealed that extremely dry years will be more frequent across California as a whole, but increases in consecutive dry years are only anticipated for SoCal by the end of the 20th century (Swain et al., 2018).

We matched monthly gridded PDSI data (Dai, 2017) to each station location and calculated probability distribution functions (PDFs) of average heatwave frequency, length, and daily mean temperature (DMT) versus two drought severity indices defined for the PDSI; mild to moderate drought ($-3 < \text{PDSI} < 0$) and severe drought ($\text{PDSI} < -3$). A paired-sample *t* test was performed to assess any statistical difference in population means for the two drought severity groups. The results in Table 3 and Figure 9 show that frequency has the most distinctive regime change between mild to moderate versus severe drought in all regions, followed by heatwave DMT, and duration. Test decision values of $h = 1$ indicate that the *t* test rejects the null hypothesis at the 5% significance level (given by p); that is, $h = 1$ indicates there was a statistically significant difference between the two populations. The inland urban and rural region heatwave metrics had the most sensitivity to drought severity indices, with frequency being the most significant for inland urban ($p = 0$, $t_{\text{stat}} = 1.73$) and rural ($p = 0$, $t_{\text{stat}} = 1.31$), respectively. While the frequency PDF for inland urban had a broad distribution spectrum, the results indicate that heatwaves have a strong probability of increasing from 4 to more than 6 per year in frequency, and from 5 to 6 days in length during severe drought conditions when compared to mild/moderate drought periods. Heatwave daily mean temperature distributions increased by 1–1.5°C during severe drought conditions for all regions. The coastal urban region had no significant change for heatwave duration but did show a weak bimodal distribution in heatwave frequency and DMT. Results indicate that severe drought conditions have a statistically significant impact on heatwave metrics for all three SoCal regions with the strongest impacts on inland urban and rural regions.

4. Summary and Conclusions

While rising trends in heatwave metrics of frequency, intensity, duration, and season length in urban areas is a global issue, it is best demonstrated at regional scales given the complex atmosphere, ocean, and land interactions driving heatwave metrics in different regions across the world. We investigated driving factors affecting trends and interannual variability in heatwave metrics using three different heatwave definitions across 61 ground stations in SoCal inland urban, coastal urban, and rural subregions from 1950–2020. The SoCal region (home to ~25 million people) is characterized by a highly complex climate affected by rapid changes that required a focused and detailed regional analysis on climate change and the impacts of extreme heat events. Our investigation describes the larger-scale and synoptic meteorological and oceanic context that sets the background behavior of heatwaves in SoCal. The findings are not applicable to the rest of California or the Western U.S., due to the distinct climate and topographical dynamics between the southern and northern regions of the state (the former as a transition between subtropics and midlatitude weather regimes).

Of the three SoCal subregions, inland urban areas were the most impacted by heatwave metrics with significant rising trends in frequency, duration, intensity, and season length, with strong correlations to an increase in nighttime mean warming. The Tmin95 heatwave definition, using nighttime temperatures exclusively, showed the strongest trends for all metrics, with frequency trends (1.4 num/dec) of almost 3 times greater than EHF (0.51 num/dec) and Tmax95 (0.5 num/dec) trends. The higher Tmin95 trends appear to be consistent with a rise in nighttime accentuated heatwaves in SoCal since the late 1990s (Gershunov et al., 2009; Gershunov & Guirguis, 2012). Because coastal heatwaves are strongly modulated by low clouds and the depth of the marine layer, increasing coastal urban heatwave frequency is likely associated with a reduction in fog and marine stratus from urbanization-induced nighttime warming (Williams et al., 2015). In urban areas, heatwaves are starting earlier and ending later in the year with the current season extending from March–September compared to May–August in the midtwentieth century. Heatwave persistence later into the year combined with an increase in mean warming have the potential to increase the intensity of wildfires by enhancing aridity and the drying of fuels (Williams et al., 2019).

Increasing trends in nighttime temperatures and humidity during heatwave events since the late 1990s are evidenced by the formation of a strong moisture anomaly source off the coast of northern Baja California

with circulation patterns transporting moisture anomalies in a NNW direction into the SoCal region. For urban regions, the recent sharp rise in trends associated with the Tmin95 heatwave definition since the early 2000s suggests an increasing trend in nighttime accentuated heatwaves in California relative to background warming. When considering the effects of humidity, heatwave minimum temperature indices have increased at a rate of $\sim 1^{\circ}\text{C}/\text{dec}$ since the 1980s and correlate in space and time with an SST warming of up to 1.5°C during heatwave events extending from coastal areas off Baja California to Santa Barbara county. Synoptic circulation patterns associated with warmer SSTs resulted in mean surface winds blowing predominately from the SSE during extreme heat events, reducing upwellings in summer months and sustaining warmer ocean waters up the west coast.

The interannual variability in heatwave events shows significant direct correlations between Pacific Decadal Oscillation (PDO) modulations and heatwave frequency and duration for urban areas, with weaker indirect correlations with ENSO variability. Coastal areas had the most significant relationships with PDO modulations accounting for 42% of variance in frequency and 46% of the variance in duration, irrespective of ENSO phase. Annual average nighttime warming and interannual variability were found to strongly correlate with increasing trends in heatwave frequency and duration over inland urban regions, with a weaker correlation over coastal areas likely due to marine cloudiness and ocean cooling effects (Schwartz et al., 2014). Analysis of two drought regimes (mild to moderate and severe) showed statistically significant differences between heatwave metrics for all three regions, with frequency being the most significantly correlated with severe droughts. The probability distribution of severe drought conditions in inland urban and rural areas indicates a strong potential of heatwaves increasing from 4 to more than 6 per year in frequency, from 5 to 6 days in duration, and $1\text{--}2^{\circ}\text{C}$ in daily mean temperature during severe drought conditions.

Although uncertainties remain on the respective contribution and/or compounding effects of driving factors affecting SoCal heatwaves dynamics, this study provides some insight into their climate drivers and underlying physical processes. A deeper understanding of these processes and the trends in heatwave metrics could not only help improve heatwave predictions but also provide risk assessments for vulnerable populations, the environment, and economy, and help to develop local adaptation and mitigation strategies toward SoCal urban resilience.

Acknowledgments

This work was carried out at the Jet Propulsion Laboratory, California Institute of Technology, under a contract with NASA. Government sponsorship acknowledged. The data sets used in this study are all publicly available with sources and citations listed in Table S1 in the supporting information.

References

- AghaKouchak, A., Cheng, L. Y., Mazdiyasni, O., & Farahmand, A. (2014). Global warming and changes in risk of concurrent climate extremes: Insights from the 2014 California drought. *Geophysical Research Letters*, 41(24), 8847–8852. <https://doi.org/10.1002/2014GL062308>
- Akbari, H. (2002). Shade trees reduce building energy use and CO₂ emissions from power plants. *Environmental Pollution*, 116, S119–S126. [https://doi.org/10.1016/s0269-7491\(01\)00264-0](https://doi.org/10.1016/s0269-7491(01)00264-0)
- Akbari, H., Pomerantz, M., & Taha, H. (2001). Cool surfaces and shade trees to reduce energy use and improve air quality in urban areas. *Solar Energy*, 70(3), 295–310. [https://doi.org/10.1016/s0038-092x\(00\)00089-x](https://doi.org/10.1016/s0038-092x(00)00089-x)
- Alexander, L. V., Zhang, X., Peterson, T. C., Caesar, J., Gleason, B., Tank, A. M. G. K., et al. (2006). Global observed changes in daily climate extremes of temperature and precipitation. *Journal of Geophysical Research*, 111(D5). <https://doi.org/10.1029/2005JD006290>
- Anderson, G. B., & Bell, M. L. (2011). Heat waves in the United States: Mortality risk during heat waves and effect modification by heat wave characteristics in 43 U.S. communities. *Environmental Health Perspectives*, 119(2), 210–218. <https://doi.org/10.1289/ehp.1002313>
- Balch, J. K., Bradley, B. A., Abatzoglou, J. T., Nagy, R. C., Fusco, E. J., & Mahood, A. L. (2017). Human-started wildfires expand the fire niche across the United States. *Proceedings of the National Academy of Sciences of the United States of America*, 114(11), 2946–2951. <https://doi.org/10.1073/pnas.1617394114>
- Baldwin, J. W., Dessy, J. B., Vecchi, G. A., & Oppenheimer, M. (2019). Temporally compound heat wave events and global warming: An emerging hazard. *Earth's Future*, 7(4), 411–427. <https://doi.org/10.1029/2018EF000989>
- Barnett, T. P., Pierce, D. W., AchutaRao, K. M., Gleckler, P. J., Santer, B. D., Gregory, J. M., & Washington, W. M. (2005). Penetration of human-induced warming into the world's oceans. *Science*, 309(5732), 284–287. <https://doi.org/10.1126/science.1112418>
- Barnett, T. P., Pierce, D. W., & Schnur, R. (2001). Detection of anthropogenic climate change in the world's oceans. *Science*, 292(5515), 270–274. <https://doi.org/10.1126/science.1058304>
- Beniston, M. (2004). The 2003 heat wave in Europe: A shape of things to come? An analysis based on Swiss climatological data and model simulations. *Geophysical Research Letters*, 31(2). <https://doi.org/10.1029/2003GL018857>
- Black, E., Blackburn, M., Harrison, G., Hoskins, B., & Methven, J. (2004). Factors contributing to the summer 2003 European heatwave. *Royal Meteorology Society Weather*, 59(8), 217–223. <https://doi.org/10.1256/wea.74.04>
- Brady, R. X., Alexander, M. A., Lovenduski, N. S., & Rykaczewski, R. R. (2017). Emergent anthropogenic trends in California Current upwelling. *Geophysical Research Letters*, 44(10), 5044–5052. <https://doi.org/10.1002/2017GL072945>
- Cayan, D. R., Redmond, K. T., & Riddle, L. G. (1999). ENSO and hydrologic extremes in the western United States. *Journal of Climate*, 12(12), 3516–3516. [https://doi.org/10.1175/1520-0442\(1999\)012<3516:eaheit>2.0.co;2](https://doi.org/10.1175/1520-0442(1999)012<3516:eaheit>2.0.co;2)
- CDC. (2013). *Climate change and extreme heat events*. Accessed on 12 September 2019. Available at www.cdc.gov/climateandhealth/pubs/ClimateChangeandExtremeHeatEvents.pdf

- Cheng, L. Y., Hoerling, M., AghaKouchak, A., Livneh, B., Quan, X. W., & Eischeid, J. (2016). How has human-induced climate change affected California drought risk? *Journal of Climate*, 29(1), 111–120. <https://doi.org/10.1175/jcli-d-15-0260.1>
- Christensen, M. W., Carrio, G. G., Stephens, G. L., & Cotton, W. R. (2013). Radiative impacts of free-tropospheric clouds on the properties of marine stratocumulus. *Journal of the Atmospheric Sciences*, 70(10), 3102–3110. <https://doi.org/10.1175/jas-d-12-0287.1>
- Clemesha, R. E. S., Guirguis, K., Gershunov, A., Small, I. J., & Tardy, A. (2018). California heat waves: Their spatial evolution, variation, and coastal modulation by low clouds. *Climate Dynamics*, 50(11–12), 4285–4301. <https://doi.org/10.1007/s00382-017-3875-7>
- Collins, D. A., Della-Marta, P. M., Plummer, N., & Trewin, B. C. (2000). Trends in annual frequencies of extreme temperature events in Australia. *Australian Meteorological Magazine*, 49(4), 277–292.
- Dai, A. (2017). *Dai Global Palmer Drought Severity Index (PDSI)*. Boulder, CO: Research Data Archive at the National Center for Atmospheric Research, Computational and Information Systems Laboratory. <https://doi.org/10.5065/D6QF8R93>
- Dousset, B., & Gourmelon, F. (2003). Satellite multi-sensor data analysis of urban surface temperatures and landcover. *ISPRS Journal of Photogrammetry and Remote Sensing*, 58(1–2), 43–54. [https://doi.org/10.1016/s0924-2716\(03\)00016-9](https://doi.org/10.1016/s0924-2716(03)00016-9)
- Dousset, B., Gourmelon, F., Laaidi, K., Zeghnoun, A., Giraudet, E., Bretin, P., et al. (2011). Satellite monitoring of summer heat waves in the Paris metropolitan area. *International Journal of Climatology*, 31(2), 313–323. <https://doi.org/10.1002/joc.2222>
- Fischer, E. M., & Schar, C. (2010). Consistent geographical patterns of changes in high-impact European heatwaves. *Nature Geoscience*, 3(6), 398–403. <https://doi.org/10.1038/ngeo866>
- Gelaro, R., McCarty, W., Suarez, M. J., Todling, R., Molod, A., Takacs, L., et al. (2017). The modern-era retrospective analysis for research and applications, Version 2 (MERRA-2). *Journal of Climate*, 30(14), 5419–5454. <https://doi.org/10.1175/jcli-d-16-0758.1>
- Gershunov, A., & Barnett, T. P. (1998). Interdecadal modulation of ENSO teleconnections. *Bulletin of the American Meteorological Society*, 79(12), 2715–2725. [https://doi.org/10.1175/1520-0477\(1998\)079<2715:imoet>2.0.co;2](https://doi.org/10.1175/1520-0477(1998)079<2715:imoet>2.0.co;2)
- Gershunov, A., Cayan, D. R., & Iacobellis, S. F. (2009). The Great 2006 Heat Wave over California and Nevada: Signal of an increasing trend. *Journal of Climate*, 22(23), 6181–6203. <https://doi.org/10.1175/2009jcli2465.1>
- Gershunov, A., & Guirguis, K. (2012). California heat waves in the present and future. *Geophysical Research Letters*, 39. <https://doi.org/10.1029/2012GL052979>
- Goodrich, G. B. (2007). Influence of the Pacific decadal oscillation on winter precipitation and drought during years of neutral ENSO in the western United States. *Weather and Forecasting*, 22(1), 116–124. <https://doi.org/10.1175/waf983.1>
- Gosling, S. N., Lowe, J. A., McGregor, G. R., Pelling, M., & Malamud, B. D. (2009). Associations between elevated atmospheric temperature and human mortality: A critical review of the literature. *Climatic Change*, 92(3–4), 299–341. <https://doi.org/10.1007/s10584-008-9441-x>
- Gosling, S. N., McGregor, G. R., & Paldy, A. (2007). Climate change and heat-related mortality in six cities Part 1: Model construction and validation. *International Journal of Biometeorology*, 51(6), 525–540. <https://doi.org/10.1007/s00484-007-0092-9>
- Grimmond, C. S. B., & Oke, T. R. (1999). Heat storage in urban areas: Local-scale observations and evaluation of a simple model. *Journal of Applied Meteorology*, 38(7), 922–940. [https://doi.org/10.1175/1520-0450\(1999\)038<0922:hsual>2.0.co;2](https://doi.org/10.1175/1520-0450(1999)038<0922:hsual>2.0.co;2)
- Guirguis, K., Basu, R., Al-Delaimy, W. K., Benmarhnia, T., Clemesha, R. E. S., Corcos, I., et al. (2018). Heat, disparities, and health outcomes in San Diego County's diverse climate zones. *Geohealth*, 2(7), 212–223. <https://doi.org/10.1029/2017GH000127>
- Guirguis, K., Gershunov, A., Tardy, A., & Basu, R. (2014). The impact of recent heat waves on human health in California. *Journal of Applied Meteorology and Climatology*, 53(1), 3–19. <https://doi.org/10.1175/jamc-d-13-0130.1>
- Guzman-Morales, J., Gershunov, A., Theiss, J., Li, H. Q., & Cayan, D. (2016). Santa Ana winds of Southern California: Their climatology, extremes, and behavior spanning six and a half decades. *Geophysical Research Letters*, 43(6), 2827–2834. <https://doi.org/10.1002/2016GL067887>
- Habeeb, D., Vargo, J., & Stone, B. (2015). Rising heat wave trends in large U.S. cities. *Natural Hazards*, 76(3), 1651–1665. <https://doi.org/10.1007/s11069-014-1563-z>
- Hajat, S., & Haines, A. (2002). Associations of cold temperatures with GP consultations for respiratory and cardiovascular disease amongst the elderly in London. *International Journal of Epidemiology*, 31(4), 825–830. <https://doi.org/10.1093/ije/31.4.825>
- Hajat, S., Kovats, R. S., Atkinson, R. W., & Haines, A. (2002). Impact of hot temperature on death in London: A time series approach. *Journal of Epidemiology and Community Health*, 56(5), 367–372. <https://doi.org/10.1136/jech.56.5.367>
- Hulley, G., Shivers, S., Wetherley, E., & Cudd, R. (2019). New ECOSTRESS and MODIS land surface temperature data reveal fine-scale heat vulnerability in cities: A case study for Los Angeles County, California. *Remote Sensing*, 11(18). <https://doi.org/10.3390/rs1182136>
- IPCC (2013). In T. F. Stocker, et al. (Eds.), *Climate change 2013: The physical science basis. Contribution of Working Group I to the Fifth Assessment Report of the Intergovernmental Panel on Climate Change*. Cambridge, UK, and New York, NY: Cambridge University Press.
- Jin, Y. F., Randerson, J. T., Faivre, N., Capps, S., Hall, A., & Goulden, M. L. (2014). Contrasting controls on wildland fires in Southern California during periods with and without Santa Ana winds. *Journal of Geophysical Research: Biogeosciences*, 119(3), 432–450. <https://doi.org/10.1002/2013jg002541>
- Jones, J. (2015). *California's most significant droughts: Comparing historical and recent conditions*. Sacramento, CA: California Department of Water Resources. https://water.ca.gov/LegacyFiles/waterconditions/docs/California_Significant_Droughts_2015_small.pdf
- Kalkstein, L. S., & Greene, J. S. (1997). An evaluation of climate/mortality relationships in large U.S. cities and the possible impacts of a climate change. *Environmental Health Perspectives*, 105(1), 84–93. <https://doi.org/10.1289/ehp.9710584>
- Keeley, J. E., Baer-Keeley, M., & Fotheringham, C. J. (2005). Alien plant dynamics following fire in Mediterranean-climate California shrublands. *Ecological Applications*, 15(6), 2109–2125. <https://doi.org/10.1890/04-1222>
- Keeley, J. E., & Syphard, A. D. (2018). Historical patterns of wildfire ignition sources in California ecosystems. *International Journal of Wildland Fire*, 27(12), 781–799. <https://doi.org/10.1071/Wf18026>
- Keggenhoff, I., Elizbarashvili, M., & King, L. (2015). Heat wave events over Georgia since 1961: Climatology, changes and severity. *Climate*, 3(2), 308–328. <https://doi.org/10.3390/cli3020308>
- Knowlton, K., Rotkin-Ellman, M., King, G., Margolis, H. G., Smith, D., Solomon, G., et al. (2009). The 2006 California heat wave: Impacts on hospitalizations and emergency department visits. *Environmental Health Perspectives*, 117(1), 61–67. <https://doi.org/10.1289/ehp.11594>
- Kozlowski, D. R., & Edwards, L. M. (2007). *An analysis and summary of the July 2006 record-breaking heat wave across the State of California*. Salt Lake City, UT: NOAA Western Regional Tech Attach, No. 07-05. https://www.cnrfc.noaa.gov/publications/heatwave_ta.pdf
- Krayenhoff, E. S., Moustaqai, M., Broadbent, A. M., Gupta, V., & Georgescu, M. (2018). Diurnal interaction between urban expansion, climate change and adaptation in U.S. cities. *Nature Climate Change*, 8(12). <https://doi.org/10.1038/s41558-018-0320-9>
- LaDochy, S., & Witiw, M. (2012). The continued reduction in dense fog in the Southern California region: Possible causes. *Pure and Applied Geophysics*, 169(5–6), 1157–1163. <https://doi.org/10.1007/s00024-011-0366-3>

- Langlois, N., Herbst, J., Mason, K., Nairn, J., & Byard, R. W. (2013). Using the excess heat factor (EHF) to predict the risk of heat related deaths. *Journal of Forensic and Legal Medicine*, 20(5), 408–411. <https://doi.org/10.1016/j.jflm.2012.12.005>
- Lau, W. K. M., & Kim, K. M. (2012). The 2010 Pakistan flood and Russian heat wave: Teleconnection of hydrometeorological extremes. *Journal of Hydrometeorology*, 13(1), 392–403. <https://doi.org/10.1175/jhm-d-11-016.1>
- Libert, J. P., Dinisi, J., Fukuda, H., Muzet, A., Ehrhart, J., & Amoros, C. (1988). Effect of continuous heat exposure on sleep stages in humans. *Sleep*, 11(2), 195–209. <https://doi.org/10.1093/sleep/11.2.195>
- Luvall, J. C., Quattrochi, D. A., Rickman, D., & Estes, M. G. Jr. (2015). Urban heat islands. In G. R. North (Ed.), *Encyclopedia of atmospheric sciences* (2nd ed., Vol. 1, pp. 310–318). Cambridge, MA: Elsevier Ltd.
- Mantua, N. J., & Hare, S. R. (2002). The Pacific decadal oscillation. *Journal of Oceanography*, 58(1), 35–44. <https://doi.org/10.1023/a:1015820616384>
- Mantua, N. J., Hare, S. R., Zhang, Y., Wallace, J. M., & Francis, R. C. (1997). A Pacific interdecadal climate oscillation with impacts on salmon production. *Bulletin of the American Meteorological Society*, 78(6), 1069–1079. [https://doi.org/10.1175/1520-0477\(1997\)078<1069:apicow>2.0.co;2](https://doi.org/10.1175/1520-0477(1997)078<1069:apicow>2.0.co;2)
- Mao, Y. X., Nijssen, B., & Lettenmaier, D. P. (2015). Is climate change implicated in the 2013–2014 California drought? A hydrologic perspective. *Geophysical Research Letters*, 42(8), 2805–2813. <https://doi.org/10.1002/2015GL063456>
- Matsueda, M. (2011). Predictability of Euro-Russian blocking in summer of 2010. *Geophysical Research Letters*, 38. <https://doi.org/10.1029/2010GL046557>
- Mazdiyasni, O., Sadegh, M., Chiang, F., & AghaKouchak, A. (2019). Heat wave intensity duration frequency curve: A multivariate approach for hazard and attribution analysis. *Scientific Reports*, 9. <https://doi.org/10.1038/s41598-019-50643-w>
- McGeehin, M. A., & Mirabelli, M. (2001). The potential impacts of climate variability and change on temperature-related morbidity and mortality in the United States. *Environmental Health Perspectives*, 109, 185–189. <https://doi.org/10.1289/ehp.109-1240665>
- McGregor, G. R., Bittner, M., Fmatthies, F., Michelozzi, P., Kovats, S., & Menne, B. (2015). *Heatwaves and health: Guidance on warning-system development*. Switzerland. https://www.who.int/globalchange/publications/WMO_WHO_Heat_Health_Guidance_2015.pdf
- Meehl, G. A., & Tebaldi, C. (2004). More intense, more frequent, and longer lasting heat waves in the 21st century. *Science*, 305(5686), 994–997. <https://doi.org/10.1126/science.1098704>
- Meehl, G. A., Tebaldi, C., Walton, G., Easterling, D., & McDaniel, L. (2009). Relative increase of record high maximum temperatures compared to record low minimum temperatures in the U. S. *Geophysical Research Letters*, 36. <https://doi.org/10.1029/2009GL040736>
- Menne, M. J., Durre, I., Vose, R. S., Gleason, B. E., & Houston, T. G. (2012). An overview of the global historical climatology network-daily database. *Journal of Atmospheric and Oceanic Technology*, 29(7), 897–910. <https://doi.org/10.1175/JTECH-D-11-00103.1>
- Merte, S. (2017). Estimating heat wave-related mortality in Europe using singular spectrum analysis. *Climatic Change*, 142(3–4), 321–330. <https://doi.org/10.1007/s10584-017-1937-9>
- Mora, C., Doussot, B., Caldwell, I. R., Powell, F. E., Geronimo, R. C., Bielecki, C. R., et al. (2017). Global risk of deadly heat. *Nature Climate Change*, 7(7). <https://doi.org/10.1038/nclimate3322>
- Moritz, M. A., Moody, T. J., Krawchuk, M. A., Hughes, M., & Hall, A. (2010). Spatial variation in extreme winds predicts large wildfire locations in chaparral ecosystems. *Geophysical Research Letters*, 37. <https://doi.org/10.1029/2009GL041735>
- Nairn, J. R., & Fawcett, R. J. B. (2015). The excess heat factor: A metric for heatwave intensity and its use in classifying heatwave severity. *International Journal of Environmental Research and Public Health*, 12(1), 227–253. <https://doi.org/10.3390/ijerph2010027>
- NHS (2016). *Weather fatalities* (p. 2016). Washington, DC: National Oceanic and Atmospheric Administration. <http://www.nws.noaa.gov/om/hazstats.shtml>
- Oliver, E. C. J., Donat, M. G., Burrows, M. T., Moore, P. J., Smale, D. A., Alexander, L. V., et al. (2018). Longer and more frequent marine heatwaves over the past century. *Nature Communications*, 9. <https://doi.org/10.1038/s41467-018-03732-9>
- Ostro, B. D., Roth, L. A., Green, R. S., & Basu, R. (2009). Estimating the mortality effect of the July 2006 California heat wave. *Environmental Research*, 109(5), 614–619. <https://doi.org/10.1016/j.envres.2009.03.010>
- Ouarda, T. B. M. J., & Charon, C. (2018). Nonstationary temperature-duration-frequency curves. *Scientific Reports*, 8. <https://doi.org/10.1038/s41598-018-33974-y>
- Palmer, W. C. (1965). Meteorological drought. In *Weather Bureau Res. Paper 45* (pp. 1–58). Washington, DC: U.S. Department of Commerce.
- Perkins, S. E., & Alexander, L. V. (2013). On the measurement of heat waves. *Journal of Climate*, 26(13), 4500–4517. <https://doi.org/10.1175/jcli-d-12-00383.1>
- Perkins, S. E., Alexander, L. V., & Nairn, J. R. (2012). Increasing frequency, intensity and duration of observed global heatwaves and warm spells. *Geophysical Research Letters*, 39. <https://doi.org/10.1029/2012GL053361>
- Pierce, D. W., Barnett, T. P., AchutaRao, K. M., Gleckler, P. J., Gregory, J. M., & Washington, W. M. (2006). Anthropogenic warming of the oceans: Observations and model results. *Journal of Climate*, 19(10), 1873–1900. <https://doi.org/10.1175/jcli3723.1>
- Polade, S. D., Gershunov, A., Cayan, D. R., Dettinger, M. D., & Pierce, D. W. (2017). Precipitation in a warming world: Assessing projected hydro-climate changes in California and other Mediterranean climate regions. *Scientific Reports*, 7. <https://doi.org/10.1038/s41598-017-11285-y>
- Reynolds, R. W., Rayner, N. A., Smith, T. M., Stokes, D. C., & Wang, W. Q. (2002). An improved in situ and satellite SST analysis for climate. *Journal of Climate*, 15(13), 1609–1625. [https://doi.org/10.1175/1520-0442\(2002\)015<1609:aiisas>2.0.co;2](https://doi.org/10.1175/1520-0442(2002)015<1609:aiisas>2.0.co;2)
- Robinson, P. J. (2001). On the definition of a heat wave. *Journal of Applied Meteorology*, 40(4), 762–775. [https://doi.org/10.1175/1520-0450\(2001\)040<0762:otdoah>2.0.co;2](https://doi.org/10.1175/1520-0450(2001)040<0762:otdoah>2.0.co;2)
- Ropelewski, C. F., & Jones, P. D. (1987). An extension of the Tahiti–Darwin southern oscillation index. *Monthly Weather Review*, 115(9), 2161–2165. [https://doi.org/10.1175/1520-0493\(1987\)115<2161:aeott>2.0.co;2](https://doi.org/10.1175/1520-0493(1987)115<2161:aeott>2.0.co;2)
- Schwartz, R. E., Gershunov, A., Iacobellis, S. F., & Cayan, D. R. (2014). North American west coast summer low cloudiness: Broadscale variability associated with sea surface temperature. *Geophysical Research Letters*, 41(9), 3307–3314. <https://doi.org/10.1002/2014GL059825>
- Semenza, J. C., Rubin, C. H., Falter, K. H., Selanikio, J. D., Flanders, W. D., Howe, H. L., & Wilhelm, J. L. (1996). Heat-related deaths during the July 1995 heat wave in Chicago. *New England Journal of Medicine*, 335(2), 84–90. <https://doi.org/10.1056/nejm199607113350203>
- Shiva, J. S., Chandler, D. G., & Kunkel, K. E. (2019). Localized changes in heat wave properties across the United States. *Earth's Future*, 7(3), 300–319. <https://doi.org/10.1029/2018EF001085>
- Soden, B. J., Held, I. M., Colman, R., Shell, K. M., Kiehl, J. T., & Shields, C. A. (2008). Quantifying climate feedbacks using radiative kernels. *Journal of Climate*, 21(14), 3504–3520. <https://doi.org/10.1175/2007jcli2110.1>

- Son, J. Y., Lee, J. T., Anderson, G. B., & Bell, M. L. (2012). The impact of heat waves on mortality in seven major cities in Korea. *Environmental Health Perspectives*, 120(4), 566–571. <https://doi.org/10.1289/ehp.1103759>
- Steadman, R. G. (1984). A universal scale of apparent temperature. *Journal of Climate and Applied Meteorology*, 23(12), 1674–1687. [https://doi.org/10.1175/1520-0450\(1984\)023<1674:ausoat>2.0.co;2](https://doi.org/10.1175/1520-0450(1984)023<1674:ausoat>2.0.co;2)
- Swain, D. L., Langenbrunner, B., Neelin, J. D., & Hall, A. (2018). Increasing precipitation volatility in twenty-first-century California. *Nature Climate Change*, 8(5). <https://doi.org/10.1038/s41558-018-0140-y>
- Swain, D. L., Tsiang, M., Haugen, M., Singh, D., Charland, A., Rajaratnam, B., & Diffenbaugh, N. S. (2014). The extraordinary California drought of 2013/2014: Character, context, and the role of climate change. *Bulletin of the American Meteorological Society*, 95(9), S3–S7.
- Taha, H. (2015). *Creating and mapping an urban heat island index for California*. Martinez, CA: Altostratus Inc.
- Tan, J. G., Zheng, Y. F., Tang, X., Guo, C. Y., Li, L. P., Song, G. X., et al. (2010). The urban heat island and its impact on heat waves and human health in Shanghai. *International Journal of Biometeorology*, 54(1), 75–84. <https://doi.org/10.1007/s00484-009-0256-x>
- Tebaldi, C., Hayhoe, K., Arblaster, J. M., & Meehl, G. A. (2006). Going to the extremes. *Climatic Change*, 79(3–4), 185–211. <https://doi.org/10.1007/s10584-006-9051-4>
- Trenberth, K. E. (2011). Changes in precipitation with climate change. *Climate Research*, 47(1–2), 123–138. <https://doi.org/10.3354/cr00953>
- Trenberth, K. E., & Fasullo, J. T. (2012). Climate extremes and climate change: The Russian heat wave and other climate extremes of 2010. *Journal of Geophysical Research*, 117, D17103. <https://doi.org/10.1029/2012JD018020>
- Trenberth, K. E., Fasullo, J. T., & Shepherd, T. G. (2015). Attribution of climate extreme events. *Nature Climate Change*, 5(8), 725–730. <https://doi.org/10.1038/nclimate2657>
- United Nations, D. o. E. a. S. A., Population Division (2015). *World population prospects: The 2015 revision, key findings and advance tables*. New York, NY: United Nations.
- Williams, A. P., Abatzoglou, J. T., Gershunov, A., Guzman-Morales, J., Bishop, D. A., Balch, J. K., & Lettenmaier, D. P. (2019). Observed impacts of anthropogenic climate change on wildfire in California. *Earth's Future*, 7, 892–910. <https://doi.org/10.1029/2019EF001210>
- Williams, A. P., Gentine, P., Moritz, M. A., Roberts, D. A., & Abatzoglou, J. T. (2018). Effect of reduced summer cloud shading on evaporative demand and wildfire in coastal Southern California. *Geophysical Research Letters*, 45(11), 5653–5662. <https://doi.org/10.1029/2018GL077319>
- Williams, A. P., Schwartz, R. E., Iacobellis, S., Seager, R., Cook, B. I., Still, C. J., et al. (2015). Urbanization causes increased cloud base height and decreased fog in coastal Southern California. *Geophysical Research Letters*, 42(5), 1527–1536. <https://doi.org/10.1002/2015GL063266>
- Wilson, L. A., Morgan, G. G., Hanigan, I. C., Johnston, F. H., Abu-Rayya, H., Broome, R., et al. (2013). The impact of heat on mortality and morbidity in the Greater Metropolitan Sydney Region: A case crossover analysis. *Environmental Health*, 12. <https://doi.org/10.1186/1476-069x-12-98>